

RESEARCH ARTICLE | DECEMBER 08 2023

# Lyapunov exponents and Lagrangian chaos suppression in compressible homogeneous isotropic turbulence

Haijun Yu (于海军) ; Itzhak Fouxon ; Jianchun Wang (王建春) ; Xiangru Li (李相茹) ; Li Yuan (袁礼) ; Shipeng Mao (毛士鹏) ; Michael Mond 

 Check for updates

*Physics of Fluids* 35, 125114 (2023)

<https://doi.org/10.1063/5.0175016>



View  
Online



Export  
Citation

CrossMark



**Physics of Fluids**  
Special Topic:  
Flow and Civil Structures

**Submit Today**



# Lyapunov exponents and Lagrangian chaos suppression in compressible homogeneous isotropic turbulence

Cite as: Phys. Fluids **35**, 125114 (2023); doi: [10.1063/5.0175016](https://doi.org/10.1063/5.0175016)

Submitted: 4 September 2023 · Accepted: 17 November 2023 ·

Published Online: 8 December 2023



View Online



Export Citation



CrossMark

Haijun Yu (于海军),<sup>1,2,a)</sup> Itzhak Fouxon,<sup>3,4,a)</sup> Jianchun Wang (王建春),<sup>5,b)</sup> Xiangru Li (李相茹),<sup>1,2,c)</sup>   
Li Yuan (袁礼),<sup>1,2,d)</sup> Shipeng Mao (毛士鹏),<sup>1,2,e)</sup> and Michael Mond<sup>3,a)</sup>

## AFFILIATIONS

<sup>1</sup>NCMIS & LSEC, Institute of Computational Mathematics and Scientific/Engineering Computing, Academy of Mathematics and Systems Science, Beijing 100190, People's Republic of China

<sup>2</sup>School of Mathematical Sciences, University of Chinese Academy of Sciences, Beijing 100049, People's Republic of China

<sup>3</sup>Department of Mechanical Engineering, Ben-Gurion University of the Negev, 84105 Beer-Sheva, Israel

<sup>4</sup>Department of Computational Science and Engineering, Yonsei University, Seoul 03722, Korea

<sup>5</sup>Department of Mechanics and Aerospace Engineering, Southern University of Science and Technology, Shenzhen 518055, People's Republic of China

<sup>a)</sup> Authors to whom correspondence should be addressed: [hyu@lsec.cc.ac.cn](mailto:hyu@lsec.cc.ac.cn); [itzhak8@gmail.com](mailto:itzhak8@gmail.com); and [mond@bgu.ac.il](mailto:mond@bgu.ac.il)

<sup>b)</sup> Electronic mail: [wangjc@sustech.edu.cn](mailto:wangjc@sustech.edu.cn)

<sup>c)</sup> Electronic mail: [lixiangru@lsec.cc.ac.cn](mailto:lixiangru@lsec.cc.ac.cn)

<sup>d)</sup> Electronic mail: [lyuan@lsec.cc.ac.cn](mailto:lyuan@lsec.cc.ac.cn)

<sup>e)</sup> Electronic mail: [maosp@lsec.cc.ac.cn](mailto:maosp@lsec.cc.ac.cn)

## ABSTRACT

We study Lyapunov exponents of tracers in compressible homogeneous isotropic turbulence at different turbulent Mach numbers  $M_t$  and Taylor-scale Reynolds numbers  $Re_\lambda$ . We demonstrate that statistics of finite-time Lyapunov exponents have the same form as that in incompressible flow due to density-velocity coupling. The modulus of the smallest Lyapunov exponent  $\lambda_3$  provides the principal Lyapunov exponent of the time-reversed flow, which is usually wrong in a compressible flow. This exponent, along with the principal Lyapunov exponent  $\lambda_1$ , determines all the exponents due to vanishing of the sum of all Lyapunov exponents. Numerical results by high-order schemes for solving the Navier–Stokes equations and tracking particles verify these theoretical predictions. We found that (1) the largest normalized Lyapunov exponent  $\lambda_1 \tau_\eta$ , where  $\tau_\eta$  is the Kolmogorov timescale, is a decreasing function of  $M_t$ . Its dependence on  $Re_\lambda$  is weak when the driving force is solenoidal, while it is an increasing function of  $Re_\lambda$  when the solenoidal and compressible forces are comparable. Similar facts hold for  $|\lambda_3|$ , in contrast to well-studied short-correlated model; (2) the ratio of the first two Lyapunov exponents  $\lambda_1/\lambda_2$  decreases with  $Re_\lambda$  and is virtually independent of  $M_t$  for  $M_t \leq 1$  in the case of solenoidal force but decreases as  $M_t$  increases when solenoidal and compressible forces are comparable; (3) for purely solenoidal force,  $\lambda_1 : \lambda_2 : \lambda_3 \approx 4 : 1 : -5$  for  $Re_\lambda > 80$ , which is consistent with incompressible turbulence studies; and (4) the ratio of dilation-to-vorticity is a more suitable parameter to characterize Lyapunov exponents than  $M_t$ .

Published under an exclusive license by AIP Publishing. <https://doi.org/10.1063/5.0175016>

## I. INTRODUCTION

Lyapunov exponents (LEs) provide a useful tool to characterize the stability of complex dynamical systems. It has been extensively used to identify chaos phenomena (e.g., the Lorenz 63 model<sup>1,2</sup>) and the so-called Lagrangian coherent structures in turbulence;<sup>3–5</sup> the latter was widely adopted in engineering applications.<sup>6–9</sup> In fluid mechanical studies of turbulence, the LEs are used both to

characterize turbulent transport and turbulence itself (see e.g., Refs. 10 and 11).

For turbulence itself, the research has been so far mostly concentrated on the principal Lyapunov exponent of the three-dimensional incompressible turbulent flow fields  $\lambda_1$  (see, e.g., Refs. 12–14). This exponent describes the asymptotic rate of divergence of two solutions of the Navier–Stokes equations that are initially almost equal.

The small difference in the initial conditions grows exponentially with time where  $\lambda_1 > 0$  provides the growth exponent. Thus,  $\lambda_1$  is a measure of the instability and complexity of the turbulence state. Recognizing that the fastest timescale of turbulence is the Kolmogorov timescale  $\tau_\eta$  (see, e.g., Ref. 15), it was estimated in Ref. 16 that  $\lambda_1 \sim \tau_\eta^{-1}$ . This prediction, which disregards intermittency, was tested in Refs. 12–14. To evolve in time the two solutions defining  $\lambda_1$ , Mohan *et al.*<sup>13</sup> determined one of them by direct numerical simulation of the incompressible Navier–Stokes equations and the other by solving the linearized perturbation equation with a Fourier–Galerkin method coupled with a third-order Runge–Kutta method for time marching. For cases with Taylor-scale Reynolds numbers in the range  $Re_\lambda \in [37, 211]$ , they found that  $\lambda_1$  increases with  $Re_\lambda$  faster than the inverse of Kolmogorov timescale  $\tau_\eta$ , cf. similar results that have been reported in Refs. 12 and 14. Hassanaly and Raman<sup>17</sup> made a significant step by determining a whole set of Lyapunov exponents as necessary to determine the Kaplan–Yorke (KY) dimension of the attractor of turbulent flow (such a set includes all positive exponents and some negative ones, and a comprehensive study of the two-dimensional case was done by Clark *et al.*<sup>18</sup>). They used a second-order pressure-correction scheme with a staggered grid. They found that the KY dimension of the incompressible turbulence attractor  $D_{KY}$  scales with the ratio of the domain size  $L$ , and the Kolmogorov scale  $\eta$  as  $D_{KY} \approx (L/\eta)^{2.8}$ , and the Lyapunov eigenvectors (LVs) get more localized as  $Re_\lambda$  increases. Localization, which was also observed in Refs. 12 and 13, signifies that the fast-growing perturbation has a spatial extent much smaller than  $L$ .

We note that due to the quadratic computational cost to calculate  $N$  Lyapunov exponents of turbulence itself with  $N$  grows very fast with Reynolds number, earlier applications of LEs on turbulence are mostly based on reduced turbulence models. In fact, the Lorenz'63 system<sup>1</sup> can be regarded as a reduced turbulence model, in which only three Fourier modes are kept by the Galerkin method to approximate the Rayleigh–Bénard convection (RBC) problem. It can generate chaotic motions but has a phase diagram that is very different from the original RBC problem.<sup>19,20</sup> A more realistic and capable reduced turbulence model is the shell model proposed by Gledzer.<sup>21</sup> The first attempts to establish the Lyapunov-Re dependence were made by Yamada and Ohkitani<sup>22–24</sup> based on shell models. This approach was later extended to elastic systems by Ray and Vincenzi.<sup>25</sup> Recent updates in this direction are the Lyapunov analysis based on Fourier-decimated turbulence<sup>26</sup> and Galerkin-truncated inviscid turbulence.<sup>27</sup> A novel property of decimation models was found by Ray:<sup>26</sup> It is possible to have nonintermittent, yet chaotic, turbulent flows, with an emergent time reversibility as the effective degrees of freedom are reduced through decimation. Conversely, the study on the Galerkin-truncated inviscid fluids by Murugan *et al.*<sup>27</sup> reveals an interesting link between the thermodynamic variables  $T$  and the maximal Lyapunov exponents, the measure of (many-body) chaos, by the relation  $\lambda_1 = \sqrt{T}$ .

We remark that probably, the most immediate quantity that remains to be studied in this direction is the backward-in-time principal Lyapunov exponent. That characterizes the divergence of solutions for backward in-time evolution, which can provide a measure of time-reversal symmetry breaking by turbulence. It would be also of interest to study how finite compressibility changes  $\lambda_1$ , by providing its dependence on the Mach number  $Ma$  (the Mach number is the ratio of the typical flow velocity and speed of sound, a measure of compressibility

that equals zero for incompressible flow). Indirectly, the study below provides information on this.

The number of the Lyapunov exponents that characterize the Navier–Stokes turbulence, which constitutes an infinite-dimensional dynamical system, is infinite. However, the effective number  $N$  of intrinsic degrees of freedom of the turbulent flow, e.g., the KY dimension, is finite<sup>28</sup> (in standard phenomenology of turbulence  $N^{4/9}$  scales linearly with the Reynolds number<sup>15</sup>). The solutions of the Navier–Stokes equations then determine trajectories in the  $N$ -dimensional space that are characterized by  $N$  Lyapunov exponents that describe the evolution of distances between infinitesimally close trajectories. The number  $N$  is influenced by intermittency and calls for further investigations.

In contrast, the LEs of small-scale turbulent transport describe the divergence of trajectories of infinitesimally close fluid particles in ordinary three-dimensional space. These trajectories are called Lagrangian trajectories, and thus, we occasionally refer to the corresponding exponents as Lagrangian LEs. There are three such exponents that describe the evolution of infinitesimal parcels of passive tracers (in practice, the largest linear size of the parcel must be much smaller than  $\eta$ ). At large times, the parcels attain the shape of an ellipsoid whose axes evolve in time exponentially with the LEs providing the growth (or decay) exponents. Thus, the Lagrangian LEs provide a robust characterization of the long-time effect of the transport of matter on the smallest scales of turbulence, below the Kolmogorov scale. The principal Lagrangian LE is positive, as that of Navier–Stokes equations, so the tracers' motion is chaotic (the so-called Lagrangian chaos).

There might be a connection between the principal Lyapunov exponent of turbulence and that of turbulent transport. Crudely, both are estimated as the inverse Kolmogorov time. Moreover, localization of the fastest-growing mode of perturbations of the Navier–Stokes equations might cause this mode to localize below  $\eta$  in the limit of large  $Re_\lambda$  and thus be determined by the small-scale turbulence similarly to Lagrangian LEs. Still, it seems that the two exponents, after multiplication by  $\tau_\eta$  have different Reynolds number dependence: the Lagrangian  $\lambda_1 \tau_\eta$  must decay with  $Re_\lambda$  for incompressible flow; see detailed discussion in Ref. 29 where the difference is explained and references therein. Further studies of the difference between the two principal exponents are necessary.

The Lagrangian LEs have been thoroughly studied for incompressible flows (see, e.g., Ref. 30). Here, the LEs were calculated based on particle tracking with a second-order predictor-correction time marching scheme and a fourth-order central finite difference for velocity gradients. Johnson and Meneveau<sup>30</sup> verified that  $\lambda_1 : \lambda_2 : \lambda_3 \approx 4 : 1 : -5$ , the ratio that has been known for some time (see Refs. 11, 30, and references therein). The exponents sum to zero so that the volume of the ellipsoid of passive particles is conserved. A remarkable property of the exponents is universality: at large  $Re_\lambda$  the dimensionless exponents  $\lambda_i \tau_\eta$  are functions of  $Re_\lambda$  only, having no dependence on the details of the forcing. The large length of the inertial interval guarantees that statistics of the flow gradients, which is a small-scale turbulence property, are independent of the details of the mechanism that stirs the large-scale turbulence.

In the case of compressible flows, much less is known and universality is more restricted. A distinction must be made here between two different types of compressible flows. The first type of compressible

flow arises as an effective description of the motion of the passive particles. Probably, the first example of such a flow was presented by Maxey<sup>31</sup> who considered the motion of weakly inertial particles passively transported by incompressible turbulence. Due to inertia, a particle cannot fully follow the transporting flow and its velocity is slightly different from that of the turbulent flow at its position. The velocity difference is proportional to the local Lagrangian acceleration so that the particle's velocity is a linear combination of the flow velocity and acceleration at its position. Thus, the particle velocity is determined uniquely by its spatial position and an effective transporting flow of particles can be introduced. This flow is compressible since the divergence of the Lagrangian accelerations' field is non-zero. Thus, the solution to the continuity equation, obeyed by the particles' concentration, is a non-constant, time-dependent inhomogeneous field. This field is passive and it does not change the flow.

The flow's independence of the solutions to the continuity equation is the benchmark of the first type of compressible flow. Since Ref. 31, many other effective flow field descriptions of particles' motion in turbulence appeared. These include particles with large inertia that sediment fast,<sup>32,33</sup> bubbles,<sup>34</sup> phytoplankton,<sup>35,36</sup> and phoretic particles.<sup>37</sup> The density of particles in all these cases has universal properties and allows a unified description.<sup>38</sup> Here, the compressible flows are generic, and hence their sum of Lyapunov exponents, providing the logarithmic rate of growth of infinitesimal volumes, is negative.<sup>39</sup> This implies that the KY dimension is smaller than the dimension of space and particles distribute over a random strange attractor with multifractal density support.<sup>40</sup> The density obeys the continuity equation, providing its singular (weak) solution. It is also observed that compressibility damps chaos: All Lagrangian LEs decrease with compressibility in a model random flow,<sup>11</sup> and cases with negative  $\lambda_1$  could be envisioned.<sup>41</sup> Whereas the Lagrangian LEs describe the motion of particles below the Kolmogorov scale, quite similar phenomena occur in the inertial range. Gawędzki and Vergassola<sup>42</sup> demonstrated for a model compressible flow that tracers explosively separate for low compressibility; however, they may collapse onto each other when compressibility is high.

The other type of compressible flow is where the transport of matter by the flow is coupled to the flow, i.e., solutions to the continuity equation actively change the flow. This includes the case of inertial particles with high concentration and also the compressible turbulence at a finite Mach number, the case with many applications on which we focus below. In compressible turbulence, the density changes must be such as to keep the pressure finite, thus avoiding infinite forces. This introduces the forbidding principle for isothermal (or any other barotropic) turbulence: Lagrangian transport may not result in infinite density or solutions to the continuity equation must remain finite and smooth.<sup>11,43</sup> In cases where both density and temperature are non-trivial, care is needed. For instance, if the ideal gas equation of state holds, then density can become infinite provided the temperature vanishes simultaneously so the product of density and temperature remains finite. In fact, this possibility is realized in fluid mechanics with cooling where density may blow up in finite time.<sup>44–46</sup> In the case of conservative hydrodynamics, we conjecture that this type of singularity may not occur and density stays finite so that

$$\lim_{t \rightarrow \infty} \frac{1}{t} \ln \left[ \frac{\rho(\mathbf{q}(t), t)}{\rho(\mathbf{q}(0), 0)} \right] = 0, \quad (1)$$

where the density field  $\rho(\mathbf{x}, t)$  is evaluated on the Lagrangian trajectory  $\mathbf{q}(t)$ . However, by mass conservation, the product of infinitesimal volume and the density is constant so the above implies that the sum of Lagrangian LEs must vanish for compressible turbulence.<sup>11</sup> The physical reasons for the vanishing are temporal anticorrelations of the flow divergence evaluated on  $\mathbf{q}(t)$  as was formalized via several identities in the main text and in the Appendix of Fouxon and Mond;<sup>43</sup> see also below. Thus, the sum of the Lyapunov exponents obtained from numerical simulations must vanish, provided that the flow gradients are fully resolved (see discussion in Ref. 43).

The conclusion on the vanishing of the sum of LEs is robust. However, Schwarz *et al.*<sup>47</sup> observed the sum to be non-zero. These authors studied the LEs of passive particles in the frame of isothermal compressible Euler equations. They adopted the CWENO scheme<sup>48</sup> for direct numerical simulation (DNS) and employed a linear velocity interpolation and a third-order strong-stability-preserving Runge–Kutta method<sup>49</sup> for particle tracking. The LEs are calculated using a standard method proposed by Benettin *et al.*<sup>50</sup> They found that the sum of LEs is not equal to 0, which implies that the KY dimension is smaller than 3 and the particles' density is a singular field supported on a multifractal. This contradiction requires an explanation and is one of the reasons for the current work, which provides seemingly the only measurement of the sum of the LEs alternative to Ref. 47.

Schwarz *et al.*<sup>47</sup> simulated the motion of passive tracers whose density does not react on the flow. In this form, their result does not contradict the forbidding principle. However, the authors claimed that the density of tracers is equal to that of the fluid, so that the fluid density is singular which does contradict the finiteness of forces in the fluid and, in fact, the continuum assumption itself. We observe that despite that both densities, that of the fluid, and that of the tracer particles, obey the continuity equation with the same flow, these densities might differ as was explained in Ref. 43. This is because the continuity equation is not dissipative and a fine difference may persist. Yet, the numerical observation of the difference is highly delicate. The result of Schwarz *et al.*<sup>47</sup> could be an observation of such a difference. Another possible explanation could be that the non-zero sum of the LEs arises in Ref. 47 because they essentially measure the coarse-grained LEs in the inertial range and not the true LEs that demand the introduction of viscosity in the numerical scheme and resolution of sub-Kolmogorov scales.

Lagrangian LEs of compressible turbulence, it seems, were studied in Ref. 47 only. These authors did not study the dependence of the LEs on the Mach and Reynolds numbers and also their results, as explained, demand a further study. For starters, a consistent study of the LEs demands determining the needed resolution and which parameters determine the exponents uniquely. Several issues arise.

Compressible turbulence is characterized by a larger number of relevant spatial scales than its incompressible counterpart. The phenomenology of incompressible turbulence operates with the energy pumping scale  $L$  and energy dissipation (Kolmogorov) scale  $\eta$  only (see, e.g., Ref. 15). Velocity is determined mainly by the flow fluctuations at the scale  $L$  and its gradients by those at the scale  $\eta$ . In compressible turbulence, there are two components to the flow, solenoidal and compressible, and their behavior can be different. Both components are excited at the scale  $L$ , either directly by forcing, or indirectly by coupling to the other component. However, the scales that determine the components' gradients might differ. Roughly speaking, gradients of the solenoidal component are determined by the size of the

smallest vortices in the flow, whereas gradients of the compressible component (the flow divergence) are determined by the smallest width of the shocks. These scales might differ. In the current work, we consider Mach numbers smaller than one so that the Kolmogorov scaling might be anticipated to describe the solenoidal component fairly well. That would imply that the smallest scale associated with this component is the Kolmogorov scale. The latter scales as  $Re^{-3/4}$ , where  $Re$  is the ordinary Reynolds number, and is the scale that determines the gradients of the solenoidal component of the flow (vorticity). On the other hand, the naive smallest scale of the shock, estimated from the Burgers-type solutions, scales proportionally to  $Re^{-1}$ . Hence, the smallest scale of the flow is anticipated to behave as  $L/Re$ . Thus, in principle, accurate determination of the flow derivatives, which is necessary to determine the LEs, demands resolution below this scale.

The LEs derive from the gradients of the flow  $\nabla \mathbf{u}$ . Hence, in computing the exponents, it is significant to understand whether the statistics of the gradients of the compressible turbulent flow are universal and what they depend on. Both, the solenoidal and the compressible components of the flow, are relevant. The sum of the Lyapunov exponents is determined by the flow divergence and thus, mostly by the compressible component of the flow. [It still has an implicit dependence on the solenoidal component via the Lagrangian trajectory on which the divergence is determined (see below).] Other combinations of the exponents, generally speaking, depend on both components. It can be hoped that if the statistics of the gradients are universal, then the Lyapunov exponents, made dimensionless by multiplying with  $\langle |\nabla \mathbf{u}|^2 \rangle^{-1/2}$  would depend only on the degree of compressibility  $C \equiv \langle (\nabla \cdot \mathbf{u})^2 \rangle / \langle |\nabla \mathbf{u}|^2 \rangle$  and the Reynolds number. The ratio  $C$  measures the compressibility of the small-scale turbulence, changing from zero for incompressible flow to one for potential flow.

The forcing that drives the turbulence imposes on the flow comparative weights of the solenoidal and compressible components at the scale  $L$ . In order to have universal statistics of the gradients, the inertial range must be as large as needed so that at the smallest scale of the flow the weights of the flow components attain intrinsic values that are independent of their values at scale  $L$ . Thus, unless the inertial range is large (larger than in the case of incompressible turbulence), the gradients and the LEs would not be universal. They would depend on  $Re$ , on  $Ma$ , and the type of force. Moreover, the dependence on  $Ma$  is non-obvious since the local Mach number associated with the small-scale turbulence is anticipated to be small in many cases. That would make small-scale turbulence effectively incompressible with all its implications. It is seen from the above that compressible turbulence imposes many issues. Some of them are tackled below.

In this paper, we investigate LEs of passive particles in three-dimensional compressible isotropic turbulence by using high-order methods for direct numerical simulation and for tracking particles, with a particular emphasis on their dependence on Taylor Reynolds number and turbulent Mach number, as well as the driving force. We check whether the sum of the LEs vanishes and whether the LEs decay as a function of the Mach number. The remaining part of the paper is presented in five sections. We first describe the governing equations and the driving force in Sec. II. Definitions and properties of the Lyapunov exponents are presented in Sec. III while Sec. IV describes the high-order numerical schemes for DNS, tracking particles, and the calculation of LEs. The major results are presented and discussed in Sec. V. Conclusions are given in Sec. VI.

## II. GOVERNING EQUATIONS

### A. Compressible Navier–Stokes equations and the driving force

We study compressible homogeneous isotropic turbulence governed by the following three-dimensional Navier–Stokes equations in a dimensionless form<sup>51</sup>:

$$\frac{\partial \rho}{\partial t} + \frac{\partial(\rho u_j)}{\partial x_j} = 0, \tag{2}$$

$$\frac{\partial(\rho u_i)}{\partial t} + \frac{\partial[\rho u_i u_j + p_m \delta_{ij}]}{\partial x_j} = \frac{1}{Re} \frac{\partial \sigma_{ji}}{\partial x_j} + \mathcal{F}_i, \tag{3}$$

$$\frac{\partial \mathcal{E}}{\partial t} + \frac{\partial[(\mathcal{E} + p_m)u_j]}{\partial x_j} = \frac{1}{\alpha} \frac{\partial}{\partial x_j} \left( \kappa \frac{\partial T}{\partial x_j} \right) + \frac{1}{Re} \frac{\partial(\sigma_{ji} u_i)}{\partial x_j} - \Lambda + \mathcal{F}_j u_j, \tag{4}$$

where  $\rho$  is the fluid density,  $u_i$  is the  $i$ th component of fluid velocity, viscous stress tensor  $\sigma_{ij} = \mu \left( \frac{\partial u_i}{\partial x_j} + \frac{\partial u_j}{\partial x_i} \right) - \frac{2}{3} \mu \theta \delta_{ij}$ , dilatation  $\theta = \partial u_i / \partial x_i$ , scaled pressure  $p_m = \frac{p}{\gamma Ma^2}$ , pressure  $p = \rho T$ , and  $\mathcal{E} = \frac{p}{(\gamma-1)\gamma Ma^2} + \frac{1}{2} \rho (u_i u_i)$  the total energy per unit volume.  $\mathcal{F}_i$  is a large-scale driving force, and  $\Lambda$  a cooling function. Einstein’s summation convention is adopted. For simplicity, Stokes’ hypothesis is assumed to be true, i.e., the bulk viscosity is set to 0. Note that the equations are nondimensionalized such that the spatial averaged density  $\langle \rho \rangle = 1$ , and the size of the computational box is a cube with side length  $L = 2\pi$ . There are three reference dimensionless parameters: the reference Mach number  $Ma = U_f / c_f$ , the reference Reynolds number  $Re = \rho_f U_f L_f / \mu_f$ , and the reference Prandtl number  $Pr = \mu_f C_p / \kappa_f$ , where  $U_f, c_f, L_f, \mu_f, \kappa_f, C_p$  are reference velocity, speed of sound, length, viscosity, thermal conductivity, and specific heat at constant pressure, respectively. The coefficient  $\alpha$  is equal to  $Pr Re (\gamma - 1) Ma^2$ . Here,  $\gamma$  is the ratio of specific heat at constant pressure  $C_p$  to that at constant volume  $C_v$ . In this study, we fix  $Pr = 0.7$  and  $\gamma = 1.4$ . The scaled  $\mu$  and  $\kappa$  satisfy the following Sutherland’s formula<sup>52</sup>:

$$\mu = \kappa = \frac{1.4042 T^{1.5}}{T + 0.40417}.$$

The cooling function takes the form  $\Lambda = aT^b$ . Several studies have shown that the statistics are not sensitive to the choice of the cooling function.<sup>51,53,54</sup> So, we fix  $b = 1$  in this paper.

The decomposition of the flow into the sum of the solenoidal and compressible components is done in the Fourier space as

$$\mathbf{v}(\mathbf{k}, t) \equiv \int_{[0,2\pi]^3} \exp(-i\mathbf{k} \cdot \mathbf{x}) \mathbf{u}(\mathbf{x}, t) d\mathbf{x}; \tag{5}$$

$$\mathbf{v}(\mathbf{k}, t) = \mathbf{v}^s(\mathbf{k}, t) + \mathbf{v}^c(\mathbf{k}, t); \quad \mathbf{v}^c = \frac{\mathbf{k}(\mathbf{k} \cdot \mathbf{v})}{|\mathbf{k}|^2}, \quad \mathbf{v}^s = \mathbf{v} - \mathbf{v}^c.$$

The solenoidal and compressible components determine the flow’s curl (vorticity) and divergence, respectively.

It is known that the statistics in (compressible) turbulence are sensitive to the driving force. Different kinds of forces have been considered in the literature, see, e.g., Wang *et al.*,<sup>51</sup> Eswaran and Pope,<sup>55</sup> Kida and Orszag,<sup>56</sup> Mininni *et al.*,<sup>57</sup> Petersen and Livescu,<sup>58</sup> Konstandin *et al.*,<sup>59</sup> and John *et al.*,<sup>60</sup> Here, we adopt a large-scale

driving force that can lead to a statistical steady state quickly.<sup>51</sup> The large-scale forcing is constructed in Fourier space by fixing  $E(k)$  within the two lowest wave number shells:  $k=1$  and  $k=2$ , where  $E(k) = \sum_{k-0.5 < |k| \leq k+0.5} |\mathbf{v}(\mathbf{k})|^2/2$ , to prescribed values that are consistent with the  $k^{-5/3}$  kinetic energy spectrum. More precisely, if a pure solenoidal force is adopted, after the forcing, we let

$$\mathbf{v}_{\text{new}}(\mathbf{k}, t) = \alpha_k \mathbf{v}^s(\mathbf{k}, t) + \mathbf{v}^c(\mathbf{k}, t), \quad (6)$$

such that the velocity magnitude in  $k=1$  and  $k=2$  shells are equal to pre-specified values  $E(k)$ ,  $k=1, 2$ . This is achieved by taking

$$\alpha_k = \sqrt{\frac{E(k) - E^c(k)}{E^s(k)}}, \quad E^\beta(k) = \sum_{k-0.5 < |k| \leq k+0.5} \frac{1}{2} |\mathbf{v}^\beta(\mathbf{k}, t)|^2, \quad (7)$$

$$\beta = c, s.$$

For forces with nonzero compressible components, we modify the compressible component as well. To this end, we use a factor  $\gamma_0$  to denote the ratio of the solenoidal part to the compressible part. The driving force is applied to obtain

$$\mathbf{v}_{\text{new}}(\mathbf{k}, t) = \alpha_k^s \mathbf{v}^s(\mathbf{k}, t) + \alpha_k^c \mathbf{v}^c(\mathbf{k}, t), \quad (8)$$

where

$$\alpha_k^s = \sqrt{\frac{\gamma_0(E(k) - E^c(k)) + E^s(k)}{(1 + \gamma_0)E^s(k)}}, \quad \alpha_k^c = \sqrt{\frac{(E(k) - E^s(k)) + \gamma_0 E^c(k)}{(1 + \gamma_0)E^c(k)}}. \quad (9)$$

In particular,

- $\gamma_0 = \infty$  generates a purely solenoidal force, the case called below ST.
- $\gamma_0 = 1$  generates a force with the solenoidal and compressible parts comparable, the case called below C1.
- $\gamma_0 = 0$  generates a force with only the compressible part.

Due to the limitation of computational resources, in this paper, we will only investigate the ST and C1 cases.

### B. Statistical quantities

The following important statistical quantities are of interest in compressible turbulence. The root mean square (rms) component fluctuation velocity  $u'$  is defined and related to the kinetic energy spectrum  $E(k)$  as

$$\frac{3}{2} (u')^2 \equiv \frac{1}{2} \langle \mathbf{u}(\mathbf{x}, t) \cdot \mathbf{u}(\mathbf{x}, t) \rangle = \int_0^\infty E(k) dk,$$

where  $\langle \cdot \rangle$  stands for the spatial average. The longitudinal integral length scale is

$$L_f = \frac{\pi}{2u'^2} \int_0^\infty \frac{E(k)}{k} dk.$$

The transverse Taylor microscale  $\lambda$  and Taylor Reynolds number  $Re_\lambda$  are defined as

$$\lambda = \frac{u'}{\langle (\partial u_i / \partial x_i)^2 / 3 \rangle^{1/2}}, \quad Re_\lambda = \frac{u' \lambda \langle \rho \rangle}{\langle \mu \rangle} Re,$$

where the summation convention is not assumed in the equation. The viscous dissipation rate  $\varepsilon$ , Kolmogorov length scale  $\eta$ , and timescale  $\tau_\eta$  are defined as

$$\varepsilon = \left\langle \sigma_{ij} \frac{\partial u_i}{\partial x_j} \right\rangle, \quad \eta = Re^{-3/4} [\langle \mu^3 \rangle / \langle \rho^2 \rangle / \varepsilon]^{1/4},$$

$$\tau_\eta = Re^{-1/2} (\langle \mu \rangle / \varepsilon)^{1/2}.$$

The turbulent Mach number  $M_t$  is defined as

$$M_t = Ma \langle u_1^2 + u_2^2 + u_3^2 \rangle^{1/2} / \langle \sqrt{T} \rangle.$$

## III. DEFINITIONS AND PROPERTIES OF LYAPUNOV EXPONENTS OF COMPRESSIBLE TURBULENCE

### A. Definitions

The trajectories of passive particles in a fluid are determined by

$$\frac{d\mathbf{q}(t)}{dt} = \mathbf{u}(\mathbf{q}(t), t), \quad \mathbf{q}(t=0) = \mathbf{q}_0, \quad \mathbf{q}(t) \in \mathbb{R}^3, \quad (10)$$

where  $\mathbf{u}$  is the flow field obtained from DNS. An infinitesimal perturbation  $\mathbf{r}_0$  in the initial condition  $\mathbf{q}(t=0) = \mathbf{q}_0 + \mathbf{r}_0$  leads to a slightly different trajectory. The distance  $\mathbf{r}(t)$  between the two resulting trajectories obeys the evolution equation

$$\frac{d\mathbf{r}(t)}{dt} = (\mathbf{r}(t) \cdot \nabla) \mathbf{u}, \quad \mathbf{r}(t=0) = \mathbf{r}_0, \quad \mathbf{r}(t) \in \mathbb{R}^3, \quad (11)$$

where the flow gradients are evaluated on the trajectory  $\mathbf{q}(t)$ . The Lyapunov characteristic number (LCN) is defined as

$$\lambda(\mathbf{q}_0, \mathbf{r}_0) = \limsup_{t \rightarrow \infty} \frac{1}{t} \frac{|\mathbf{r}(t)|}{|\mathbf{r}_0|}. \quad (12)$$

It has the following basic property: there exist  $d$  linear subspaces  $Z_d \subset Z_{d-1} \subset \dots \subset Z_1 = \mathbb{R}^d$ , such that

$$\lambda_i(\mathbf{q}_0) = \max_{\mathbf{r}_0 \in Z_i} \lambda(\mathbf{q}_0, \mathbf{r}_0) = \{ \lambda(\mathbf{q}_0, \mathbf{r}_0); \forall \mathbf{r}_0 \in Z_i \setminus Z_{i+1} \}.$$

Alternatively, we may define Lyapunov exponents using the Cauchy-Green tensor. Consider

$$\frac{dD_{ij}(t)}{dt} = \frac{\partial u_i}{\partial x_k}(\mathbf{q}(t), t) D_{kj}(t), \quad D_{ij}(t=0) = \delta_{ij}. \quad (13)$$

The finite-time Lyapunov exponents (FTLEs) are defined by using the singular values  $\sigma_i(\mathbf{q}_0, t)$  of the deformation tensor  $D_{ij}$ , i.e., the square roots  $\sigma_i$  of the eigenvalues of the symmetric positive Cauchy-Green tensor  $C_{ij} = D_{ik} D_{jk}$ ,

$$\gamma_i(\mathbf{q}_0, t) := \frac{1}{t} \ln \sigma_i(\mathbf{q}_0, t).$$

The Lyapunov exponents (LEs) are defined as the infinite time limit of FTLEs and are equivalent to LCNs, i.e.,

$$\lim_{t \rightarrow \infty} \gamma_i(\mathbf{q}_0, t) = \lambda_i(\mathbf{q}_0). \quad (14)$$

### B. Representation of the Lyapunov exponents for three-dimensional flow

We are concerned with three-dimensional flows where the spectrum of the Lyapunov exponents is fully described by  $\lambda_1, \lambda_3$ , and  $\sum_{i=1}^3 \lambda_i$ . These three quantities allow a simplified description in any

dimension. Considering  $\mathbf{q}(t)$  as a vector function of the initial condition  $\mathbf{q}_0$ , we find from Eq. (13) that the Jacobi determinant of this function,  $J(t) = |\partial\mathbf{q}(t)/\partial\mathbf{q}_0|$ , obeys a simple equation. We have by using the definition of  $\lambda_i$ ,

$$\frac{d \ln J(t)}{dt} = \nabla \cdot \mathbf{u}, \quad \sum \lambda_i \equiv \lim_{t \rightarrow \infty} \frac{\ln J(t)}{t} = \lim_{t \rightarrow \infty} \frac{1}{t} \int_0^t \langle \nabla \cdot \mathbf{u}(\mathbf{q}, t') \rangle_L dt', \quad (15)$$

where  $\langle \cdot \rangle_L$  denotes the Lagrangian average. Ergodicity is assumed which will be numerically verified in Sec. VC. Due to the fact that  $\frac{d}{dt} \ln \rho(\mathbf{q}, t) = -\nabla \cdot \mathbf{u}$ , we also have

$$\sum \lambda_i = \lim_{t \rightarrow \infty} \frac{1}{t} \int_0^t -\frac{d}{dt} \ln \rho(t') dt' = \lim_{t \rightarrow \infty} \frac{1}{t} (\ln \rho(0) - \ln \rho(t)). \quad (16)$$

If we take uniform initial density, i.e.,  $\rho(0) \equiv 1$ , then we have

$$\sum \lambda_i = \lim_{t \rightarrow \infty} -\ln \rho(t)/t = \lim_{t \rightarrow \infty} -\langle \ln \rho(t) \rangle_L / t. \quad (17)$$

Since  $\langle \cdot \rangle_L$  denotes the Lagrangian average and the passive particles and the fluid density have the same probability distribution in a statistically steady turbulence state,  $\langle \ln \rho(t) \rangle_L = \langle \rho(t) \ln \rho(t) \rangle \geq \langle \rho(t) \rangle \ln \langle \rho(t) \rangle = 0$  by Jensen inequality. Here, the assertion that Lagrangian averages are equivalent to density-weighted averages is assumed and will be justified by a numerical investigation given in Sec. VC. Thus, if the startup density satisfies a uniform distribution, then the sum of finite time LEs will take negative values and converge to 0 from below at a speed  $\mathcal{O}(1/t)$ .

For the largest and smallest LEs, they can be evaluated using the following dynamics<sup>10,11</sup>:

$$\lambda_1 = \lim_{t \rightarrow \infty} \frac{1}{t} \int_0^t \sigma : \mathbf{r}_1 \mathbf{r}_1 dt', \quad \frac{d\mathbf{r}_1}{dt} = \sigma \cdot \mathbf{r}_1 - (\sigma : \mathbf{r}_1 \mathbf{r}_1) \mathbf{r}_1, \quad (18)$$

$$\lambda_3 = \lim_{t \rightarrow \infty} \frac{1}{t} \int_0^t \sigma : \mathbf{r}_3 \mathbf{r}_3 dt', \quad \frac{d\mathbf{r}_3}{dt} = -\sigma^T \cdot \mathbf{r}_3 + (\sigma : \mathbf{r}_3 \mathbf{r}_3) \mathbf{r}_3, \quad (19)$$

where  $\sigma = \nabla_x \mathbf{u}$  and  $\mathbf{r}_1, \mathbf{r}_3$  are two randomly initialized vectors in the respective linear subspaces (e.g.,  $\mathbf{r}_I(0) \in Z_1 \setminus Z_2$ ). We note that Eq. (18) is mathematically equivalent to Eqs. (11) and (12), so we can use Eq. (25) below to estimate it. Equation (19) is obtained in Appendix B of Balkovsky and Fouxon.<sup>10</sup> Roughly speaking, the representation for  $\lambda_3$  can be explained by observing that the equation on the Cauchy–Green tensor, which in matrix form reads  $\dot{D} = \sigma D$ , implies  $\dot{D}^{-1,T} = -\sigma^T D^{-1,T}$ . The singular values of  $D^{-1,T}$  are  $-\lambda_i$ , which implies Eq. (19). Since Eqs. (18) and (19) have similar forms, we can use the standard numerical method for  $\lambda_1$  to calculate  $\lambda_3$  by considering the transformed backward dynamics.

### C. Incompressible-like large deviations theory of finite-time Lyapunov exponents

We saw that  $\sum \lambda_i$  of compressible turbulence equals zero as in the incompressible flow. We demonstrate here that fluctuations of the finite-time Lyapunov exponents also behave as in the incompressible flow. This has a remarkable consequence that  $|\lambda_3|$  is the first Lyapunov exponent of the time-reversed flow. In general, an infinitesimal spherical parcel of the fluid is transformed by the flow into an ellipsoid, whose largest and smallest axes, asymptotically at large times, grow

and shrink exponentially, with exponents  $\lambda_1$  and  $\lambda_3$ , respectively. Reversing this evolution naively, we find that in time-reversed flow the stretching occurs with exponent  $|\lambda_3|$  and shrinking with the exponent  $-\lambda_1$ . In fact, this consideration is generally true in incompressible flow only: Compressibility introduces a non-trivial Jacobian (volume) factor, which usually depends on time exponentially causing the principal exponent of the time-reversed flow to differ from  $|\lambda_3|$  (see the arXiv version of Balkovsky *et al.*<sup>61</sup>). In compressible turbulence, however, the Jacobian is stationary since infinitesimal volumes define stationary density. This makes the volume factor irrelevant to the exponential behavior of the ellipsoid’s dimensions.

We provide a more formal description of the considerations above. We consider the joint probability density function (PDF) of

$$\begin{aligned} \kappa(t) &\equiv \ln \left( \frac{\rho(0)}{\rho(\mathbf{q}(t), t)} \right) = \int_0^t \nabla \cdot \mathbf{u}(\mathbf{q}, t') dt', \\ \rho_1(t) &= \int_0^t \sigma : \mathbf{r}_1 \mathbf{r}_1 dt', \quad \rho_3(t) = \int_0^t \sigma : \mathbf{r}_3 \mathbf{r}_3 dt', \end{aligned} \quad (20)$$

where  $\mathbf{r}_{1,3}$  are defined in Eq. (19).

At large times, the distribution of  $\kappa(t)$  becomes stationary since it becomes a difference of two independent stationary processes  $\ln \rho(0)$  and  $\ln \rho(\mathbf{q}(t), t)$ . The time integral in the definition of  $\kappa(t)$  does not accumulate with time due to the anticorrelations in the temporal behavior of  $\nabla \cdot \mathbf{u}(\mathbf{q}, t)$  that manifests via the vanishing of  $\int \langle \nabla \cdot \mathbf{u}(\mathbf{q}, t) \nabla \cdot \mathbf{u}(\mathbf{q}, t') \rangle dt'$ . The vanishing of this integral in several forms (quasi-Eulerian and Lagrangian) was discussed at length in Appendix A of Fouxon and Mond.<sup>43</sup> Thus,  $\kappa(t)$  depends only on the values of the velocity divergence in the time vicinity of times 0 and  $t$  whose size is of the order of the correlation time of  $\nabla \cdot \mathbf{u}(\mathbf{q}, t)$ .

In contrast,  $\rho_{1,3}$  depends on the gradients during the entire time interval  $(0, t)$ . At large times, the contribution of time intervals near 0 and  $t$  that determine  $\kappa(t)$  can be neglected in  $\rho_{1,3}(t)$ . We infer from this that  $\kappa(t)$  and  $\rho_{1,3}(t)$  become independent (see similar considerations in Balkovsky and Fouxon<sup>10</sup>). We conclude that the joint PDF  $P(\kappa, \rho_1, \rho_3, t)$  of  $\kappa(t)$  and  $\rho_{1,3}(t)$  reads

$$P(\kappa, \rho_1, \rho_3, t) \sim P_0(\kappa) \exp \left( -tS \left( \frac{\rho_1}{t} - \lambda_1, \frac{\rho_3}{t} - \lambda_3 \right) \right), \quad (21)$$

where the standard large deviations form is used for the PDF of  $\rho_{1,3}(t)$  (see, e.g., Balkovsky and Fouxon<sup>10</sup>). The convex large deviation function  $S(x_1, x_2)$  is non-negative and it has a unique minimum of zero at  $x_1 = x_2 = 0$ . It is readily seen that at  $t \rightarrow \infty$ , the above distribution becomes a  $\delta$ -function, which guarantees that the limits in Eqs. (18) and (19) are non-random. The typical values of  $\rho_{1,3}(t)$  scale linearly with  $t$  so that at large times bounded fluctuations of  $\kappa$  become negligibly small, compared with the spread of the distribution. For most relevant observables, such as those considered in turbulent mixing,<sup>10</sup> the results of the averaging with the PDF in Eq. (21) coincide with those obtained by using the effective PDF given by

$$P(\kappa, \rho_1, \rho_3, t) \sim \delta(\kappa) \exp \left( -tS \left( \frac{\rho_1}{t} - \lambda_1, \frac{\rho_3}{t} - \lambda_3 \right) \right). \quad (22)$$

This has the same form as in the incompressible flow, as explained at the beginning of this section. The recalculation of this result into the statistics of the finite time Lyapunov exponents is straightforward (see Ref. 62). The form of the statistics is the same as in the incompressible

flow, as derived in Ref. 10. We conclude that long-time statistics of the finite-time Lyapunov exponents have the same form as in the incompressible flow. For instance, this implies that the principal Lyapunov exponent of the time-reversed flow is  $|\lambda_3|$ , and the fact that is non-true for a general compressible flow.<sup>61</sup>

**D. Perturbation theory for Lyapunov exponents at small Mach number**

We discuss here the dependence of  $\lambda_i$  on the Mach number  $Ma$ . In the limit of very small  $Ma$ , the results must be describable by the perturbation theory around the exponents of the incompressible turbulent flow that holds at  $Ma \rightarrow 0$ .<sup>53,63–66</sup> The corrections to the exponents of incompressible turbulence are of the same order in  $Ma$  as the compressible component. However, this perturbation theory holds only at very small Mach numbers, empirically below 0.1<sup>53,66</sup> and it is of no use below where larger  $Ma$  are considered.

**IV. NUMERICAL METHODS**

**A. Numerical methods for direct numerical simulation of turbulence**

We use a hybrid WENO-central compact difference method proposed by Liu *et al.*,<sup>54</sup> which is an improved version of Wang *et al.*<sup>51</sup> for DNS of compressible isotropic turbulence. The DNS solver has the following properties:

- An eighth-order compact central difference scheme (CCD8<sup>67</sup>) for smooth regions, a seventh-order WENO scheme (WENO7<sup>68</sup>) for shock regions is used to discretize the convection terms.
- Shock fronts are determined by  $\theta < -R_0\theta'$ , where  $R_0 = 3$ ,  $\theta'$  is the rms of  $\theta$ .
- Viscous dissipation terms are handled by a non-compact sixth-order central difference scheme (CD6).
- Thermal diffusion term in the energy equation is discretized using a non-hybrid CCD8 scheme.
- Strong-stability preserving third-order Runge–Kutta method (SSP-RK3<sup>49</sup>) is used for time marching.
- Numerical hyperviscosity is applied to  $\rho, u, v, w, T$  in every five steps (filtering) as

$$\frac{\partial f}{\partial t} = \nu_n [f''_n - (f'_n)'_n], \tag{23}$$

where  $f$  stands for any of  $\rho, u, v, w$ , and  $T$ , and  $f'_n, f''_n$  stands for numerical discretizations for  $f_x$  and  $f_{xx}$  using CCD8 scheme, respectively. We set  $\nu_n = 2 \times 10^{-2}$  in the numerical simulation. Note that<sup>51</sup>

$$\nu_n [f''_n - (f'_n)'_n] \sim \nu_n C(0) (\Delta x)^8 (\nabla^2)^5 f, \quad C(0) \approx 2.88 \times 10^{-5}.$$

So,  $\nu_n C(0) \ll \mu/Re$ . Thus, the numerical hyperviscosity only has a strong smoothing effect on high wave number parts. The smoothing effect on low-frequency part  $\hat{f}_k, k < k_{max}/2$  is quite small compared to the physical diffusion  $\frac{\mu}{Re} \nabla^2 f$  in the Navier–Stokes equation.

To get reliable results of Lyapunov exponents, we will only consider the cases where the shock scales can be resolved or nearly resolved numerically, which means that we focus on low Reynolds number cases. For these low Reynolds cases, we will also present numerical results computed by using a fifth-order upwind compact scheme<sup>69</sup>

together with a compact central difference scheme with hyperviscosity for comparison.

**B. Numerical methods for passive particles and Lyapunov exponents**

The standard method for numerically calculating all LEs<sup>50</sup> is described below. The method of computing all LEs needs first to choose random vectors  $\mathbf{r}_1^0, \dots, \mathbf{r}_m^0 \in \mathbb{R}^d$  with  $(\mathbf{r}_i^0, \mathbf{r}_j^0) = \delta_{ij}, m \leq d$ , then evolve them via Eq. (11), then the LEs are formally given by

$$\lambda_p = \lim_{k \rightarrow \infty} \frac{1}{k\tau} \sum_{i=1}^k \ln r_p^{(i)}, \quad r_p^{(i)} = |\tilde{\mathbf{r}}_p(\mathbf{r}_p^{(i-1)}, \tau)|, \quad p = 1, \dots, \tag{24}$$

Here,  $\mathbf{r}_p(\mathbf{r}_p^{(i-1)}, \tau)$  stands for the vector obtained by marching Eq. (11) with an initial value  $\mathbf{r}_p^{(i-1)}$  for a time period  $\tau$ .  $\tilde{\mathbf{r}}_p, p = 1, \dots, d$  are vectors after applying Gram–Schmidt orthogonalization (but not normalized) to  $\mathbf{r}_p$ . More precisely,

$$\tilde{\mathbf{r}}_p = \mathbf{r}_p - \sum_{j=1}^{p-1} (\mathbf{r}_p, \mathbf{r}_j^{(i)}) \mathbf{r}_j^{(i)}, \quad \mathbf{r}_p^{(i)} = \tilde{\mathbf{r}}_p / |\tilde{\mathbf{r}}_p|, \quad p = 1, \dots, m.$$

We note that there exist some improvements in the orthogonalization procedure (see, e.g., Ref. 70), but the standard Gram–Schmidt orthonormalization is good enough for our purpose since we only need to compute three LE exponents.

Numerically, we cannot solve the perturbation equation (11) for an infinitely long time to obtain the  $\lambda_p$  defined by Eq. (24). Instead, we will use a relatively large terminal time  $t$  and use the corresponding FTLEs to approximate LEs. The FTLEs are evaluated as

$$\gamma_p = \frac{1}{K - K_0} \sum_{i=K_0}^{K-1} a_p^{(i)}, \quad p = 1, 2, 3, \tag{25}$$

where  $a_p^{(i)} = \frac{1}{\tau} \ln r_p^{(i)}, \tau = t/K$ .  $K_0$  is a parameter to be tuned to get faster convergence by discarding data from a transient region.

To verify the numerical accuracy of the standard numerical methods for LEs, we also implemented alternative approaches (16) for the sum of all LEs and a different approach (19) for the largest and smallest LE.

**V. NUMERICAL RESULTS AND DISCUSSION**

**A. Verifying the numerical schemes**

**1. Checking numerical resolutions of DNS**

To check if the shocks are resolved by the numerical experiments, we first run a testing case using the hybrid scheme<sup>54</sup> with  $128^3$  grids for 20 time units. Then, use the solution as the initial condition and run with resolutions using  $128^3, 256^3$ , and  $512^3$  grid points, for a short time, e.g., 0.1 time unit (which is approximately equal to 1 Kolmogorov timescale). The results are reported in Figs. 1 and 2. These figures show that all the solutions are very accurate for the density and velocity fields except for some locations with huge gradients, which occupy only a small portion of the total computational domain.

For the solenoidal forcing (ST) case (Fig. 1), we see that the  $128^3$  resolution does a decent job, except for the place where  $u_x$  is smaller than  $-5$ , which corresponds to a shock wave. Notice that the shock calculated by  $128^3$  resolution is a little bit wider and less steep than that obtained using  $256^3$  and  $512^3$  resolutions.

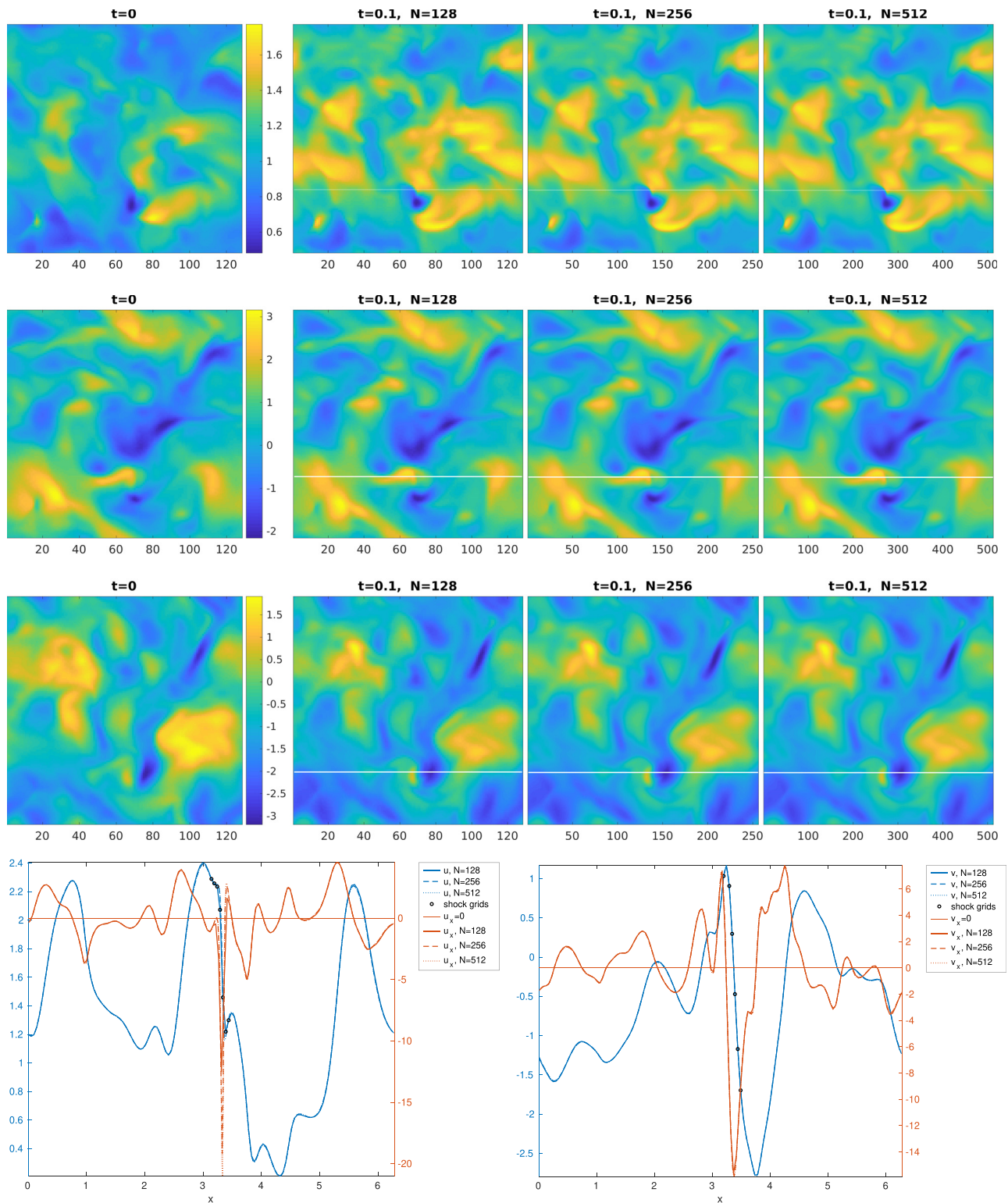
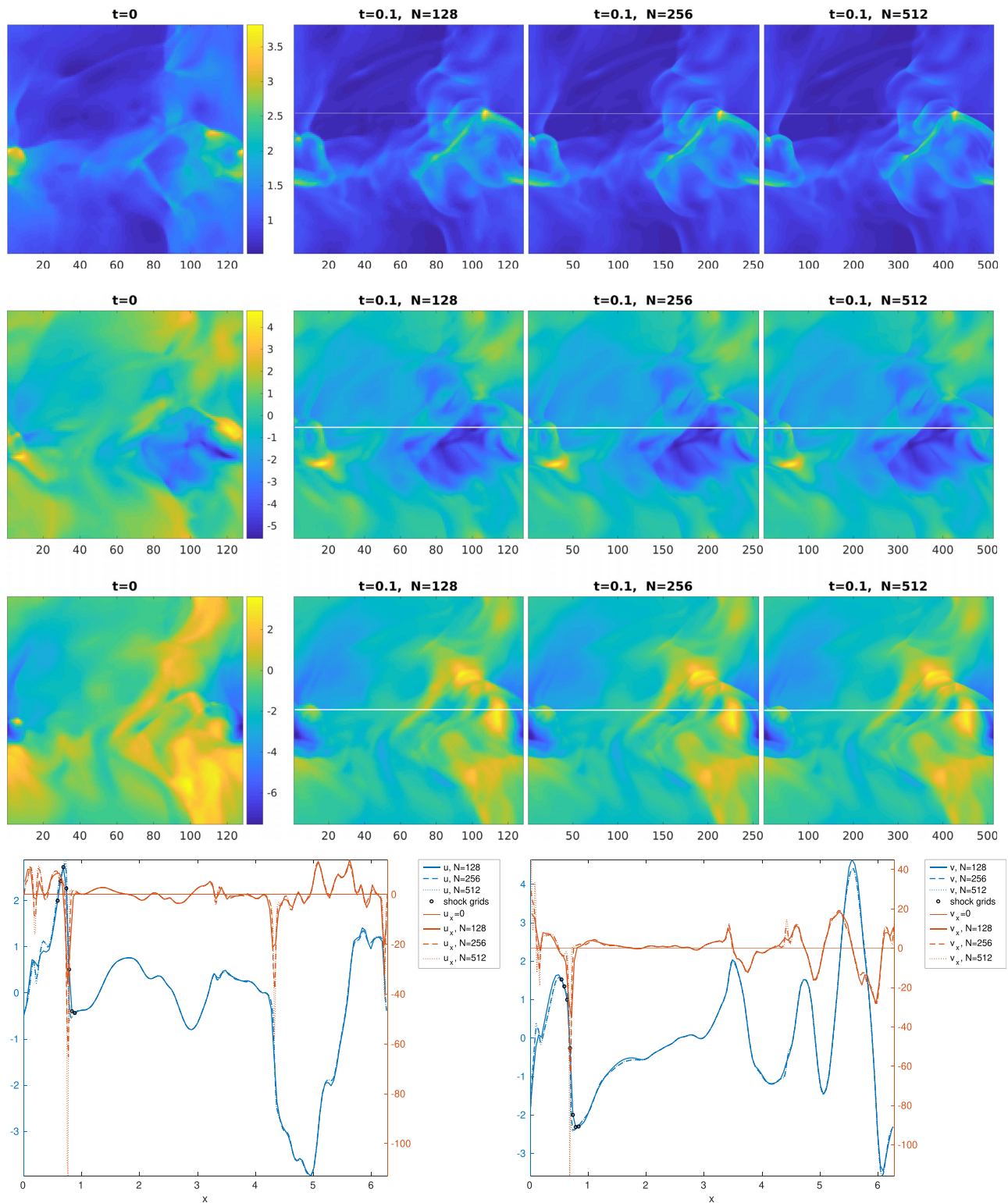
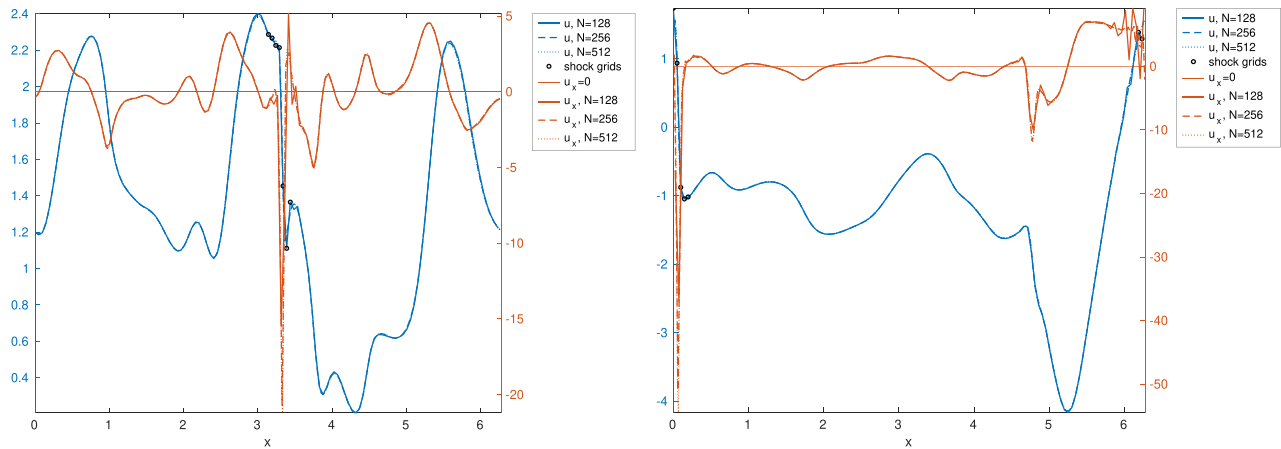


FIG. 1. Density and velocity profiles using different resolutions (ST,  $Re_\lambda = 80$ ,  $M_t = 0.8$ , hybrid scheme). From top to bottom: snapshots of  $\rho$ ,  $u$ , and  $v$  at a fixed  $z$  slice and profiles along white lines in  $u$  and  $v$  slices.



**FIG. 2.** Density and velocity fields using different resolutions (C1,  $Re_\lambda = 80$ ,  $M_t = 0.8$ , hybrid scheme). From top to bottom: snapshots of  $\rho$ ,  $u$ ,  $v$  and profiles along the white lines in  $u$  and  $v$  slices.



**FIG. 3.** Resolution check ( $u$   $x$ -profile) using compact difference scheme. Left: ST forcing,  $Re_\lambda = 80, M_t = 0.8$ : acceptable results; right: C1 forcing,  $Re_\lambda = 40, M_t = 0.4$ : oscillation happened for  $u_x$  near  $x = 6$ .

The result of the C1 forcing case (Fig. 2) is similar to the ST case. However, we see larger errors in the  $128^3$  grid case compared to the reference solution obtained by using  $512^3$  grid points, at places where gradients are large. So, we use  $256^3$  grid points for most of the numerical experiments.

In Fig. 3, we present the results of using a compact central difference scheme for a solenoidal forcing case and a mixed forcing case. We see that the compact difference scheme has better resolutions of shock thickness, but its solution has nonphysical oscillations near the rear boundaries of the shocks. For this reason, we will not use this scheme to generate DNS data.

**2. High-order schemes are necessary for calculating LEs**

There are several numerical methods that are used for evaluating LEs of passive particles in turbulence. To make a proper choice, we

tested two such schemes with different spatial and temporal discretization orders. For the low-order scheme (LS1, L stands for Lyapunov), we use a second-order central difference scheme to evaluate the velocity gradient tensor  $\nabla u$ , then carry out linear interpolation to get values on Lagrangian points and use a second-order Crank–Nicolson scheme for marching the perturbation equation (11). For the high-order scheme (LS2), we use a fourth-order central difference for  $\nabla u$  and then use cubic interpolation to get values on Lagrangian points, and a third-order Runge–Kutta<sup>49</sup> is adopted to march Eq. (11).

In Fig. 4, we present these results for a C1 forcing case with  $M_t \approx 0.8, Re_\lambda \approx 100$ , where we observe that the lower-order scheme and the high-order scheme generate results with observable differences in  $128^3$  grid resolution. By taking the computed LEs of the high-order scheme with  $256^3$  grid points as reference solutions, we see that the lower order scheme leads to large numerical errors in the computation

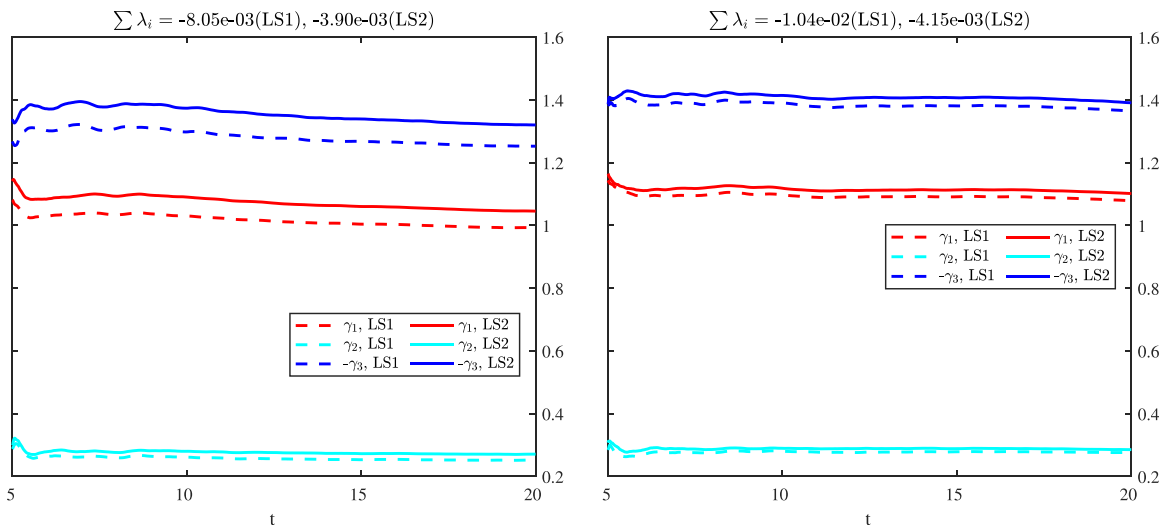


**FIG. 4.** LE results obtained with different schemes for calculating  $\sigma = \nabla_x u$  and for time marching of perturbing vectors (C1 forcing case with  $M_t \approx 0.8, Re_\lambda \approx 100$ ). Left:  $128^3$  DNS grids and right:  $256^3$  DNS grids.

12 December 2023 01:59:48

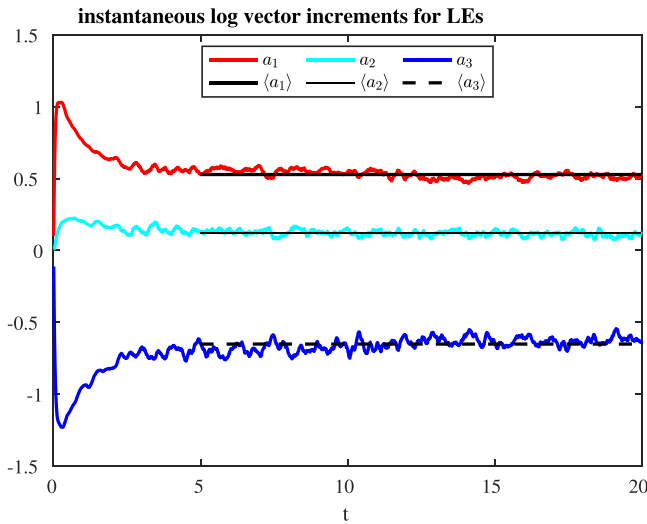


**FIG. 5.** Results of instantaneous log vector length increments  $a_p^{(i)}$  used in (25) for calculating FTLEs in a mixed-type forcing (C1) case with  $Re_\tau = 40$ ,  $Mt = 0.4$ . In this figure,  $\langle \cdot \rangle$  stands for the time average for  $t > 5$ .

of LEs. We also observed that the high-order method (LS2) leads to significantly smaller values of the sum of LEs. For this reason, we adopt the high-order scheme in the remaining part of this paper. We also note that the sum of LEs in the  $256^3$  grid case is larger than the case with the  $128^3$  grid case. However, this difference is insignificant compared to the differences in LEs themselves. As shown by Eqs. (16) and (17), the sum of finite time LEs usually takes negative values and converges to 0 from below at a speed  $O(1/t)$ . The small difference is due to the fluctuations in the Lagrangian-averaged density at the start and terminal time.

### 3. Remove the dependence on initial conditions

For the initial condition of the DNS, we use uniform density  $\rho(x, 0) \equiv 1$ , uniform temperature  $T(x, 0) \equiv 1$ , and a randomly initialized velocity field that is consistent with the  $k^{-5/3}$  scaling law. We use a uniform initial distribution for the passive particles to calculate LEs. However, there is a noticeable transient region in the first several time units, as shown in Fig. 5. Since we are interested in the properties of the statistical steady state, we expect to obtain more physical and accurate results by removing the initial transient region related to the initial conditions. To this end, we tested doing particle tracking from  $t_0 \approx 3T_e$ , where  $T_e = L_f/u'$  is the large-eddy turnover time. However, the numerical results are similar to the ones without discarding the transient region of the flow. We also tried doing particle tracking from the very beginning but evaluating finite-time Lyapunov exponents from  $t_0 \approx 3T_e$ , which is equivalent to replacing the summation  $i = 1$  by  $i = t_0/\tau$  in (24) or setting  $K_0 = t_0/\tau$  in Eq. (25). By doing this, the relaxation periods of both DNS and the LE dynamics are removed, and a faster convergence is observed (see Fig. 6). In this figure, calculated FTLEs as functions of time using different methods are plotted. The FTLEs at the largest simulated time are taken as estimates of LEs. The red, green, and blue curves are three FTLEs calculated using three tracked vectors with Gram-Schmidt orthonormalization at each time step. The one marked by blue dots is the negative of  $\gamma_3$  obtained using a method similar to the one to the largest FTLE, but with the evolution tensor  $\sigma = \nabla \mathbf{u}$  replaced by  $\sigma = (-\nabla \mathbf{u})^t$ . The figure shows that the  $\lambda_3$  calculated using two different methods agree with each other very well. The sum of FTLEs converges to 0, which asserts that the sum of LEs is 0, despite some minor oscillations existing in the initial transient region.

We further run some typical cases using  $128^3$  and  $256^3$  grid resolutions with different DNS schemes to check the effect of numerical resolutions and schemes of DNS on the calculation of LEs. The

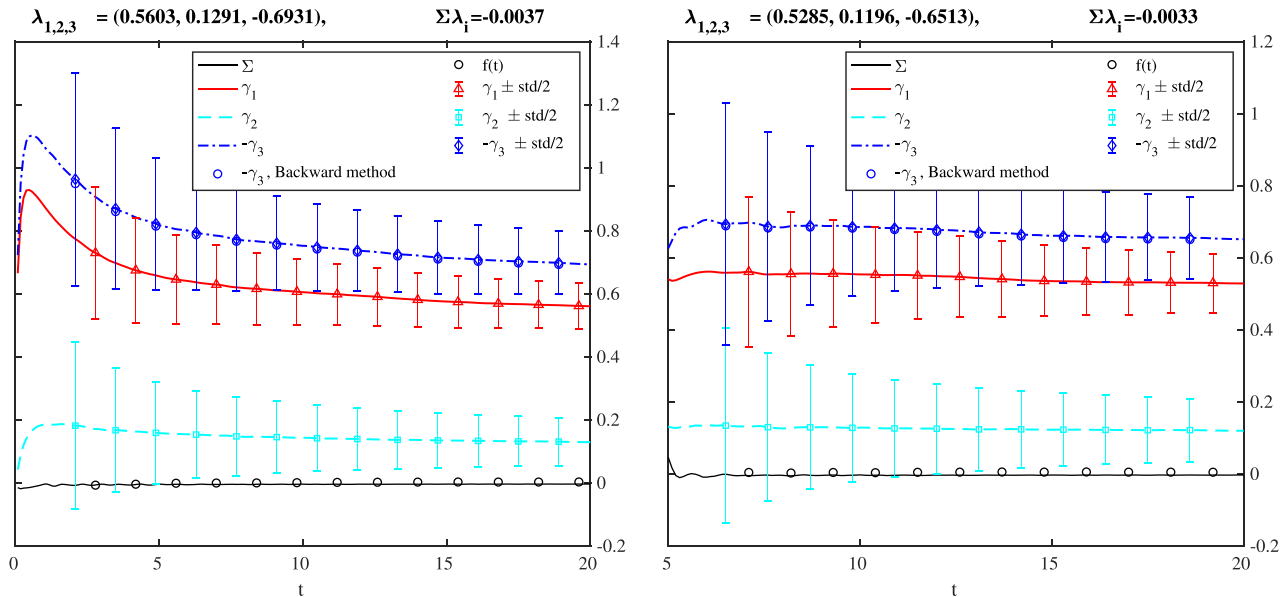


**FIG. 6.** Results of FTLEs calculated by discarding (right:  $t_0 = 5$ ) or not discarding (left:  $t_0 = 0$ ) the relaxation period. The results for a typical mixed-type forcing (C1) case with  $Re_\tau = 40$  and  $Mt = 0.4$  is shown.

**TABLE I.** Summary of results using different schemes and grid sizes. ST stands for the solenoidal driving force. C1 stands for the force with comparable solenoidal and compressible parts ( $\gamma_0 = 1$ ).

Force-scheme	Grid	$Re_L$	$Re_\lambda$	$M_t$	$\eta$	$\tau_\eta$	$\lambda_1$	$\lambda_2$	$\lambda_3$	$\lambda_1/\lambda_2$
ST-hybrid	$128^3$	1395.43	79.81	0.7961	0.0353	0.1307	0.8620	0.2130	-1.0761	4.047
ST-unwind	$128^3$	1402.75	78.36	0.8007	0.0349	0.1281	0.8801	0.2176	-1.0997	4.045
ST-hybrid	$256^3$	1407.12	81.11	0.8001	0.0346	0.1293	0.8660	0.2151	-1.0817	4.027
ST-upwind	$256^3$	1400.49	79.19	0.7988	0.0350	0.1286	0.8592	0.2154	-1.0763	3.989
C1-hybrid	$128^3$	628.48	39.84	0.4042	0.0603	0.1842	0.5763	0.1328	-0.7117	4.340
C1-upwind	$128^3$	627.46	38.04	0.4036	0.0595	0.1796	0.5673	0.1303	-0.7007	4.354
C1-hybrid	$256^3$	627.73	37.92	0.4036	0.0594	0.1787	0.5635	0.1302	-0.6976	4.328
C1-upwind	$256^3$	627.87	37.14	0.4037	0.0589	0.1762	0.5628	0.1318	-0.6995	4.270

parameters and results are summarized in Table I, from which, we see the maximum relative differences of  $\lambda_1/\lambda_2$  and  $\lambda_3$  in difference resolutions/schemes are less than 2.2%. We note that the grid size  $\Delta x$  for  $128^3$  and  $256^3$  are close to 0.049 and 0.024, respectively, which are smaller than the standard  $\Delta x \approx 2\eta$  used in the existing DNS studies.<sup>53,60</sup>

### B. Comparing the average of velocity divergence weighted by fluid density and particle number density

The quantities of  $\int_\Omega \rho \nabla \cdot \mathbf{u} \, dx$  and  $\int_\Omega n(\mathbf{x}) \nabla \cdot \mathbf{u} \, dx$  as functions of time  $t$  are plotted in Fig. 7, where  $n(\mathbf{x})$  is the number density of passive particles. We see that the two quantities agree with each other in both solenoidal and mixed forcing cases.

### C. A direct comparison of fluid density and particle number density

We next present a direct numerical study to check if the fluid density  $\rho$  and particle number density  $n$  have the same invariant distribution since they are related to the statistics of LEs. We adopt the following strategy.

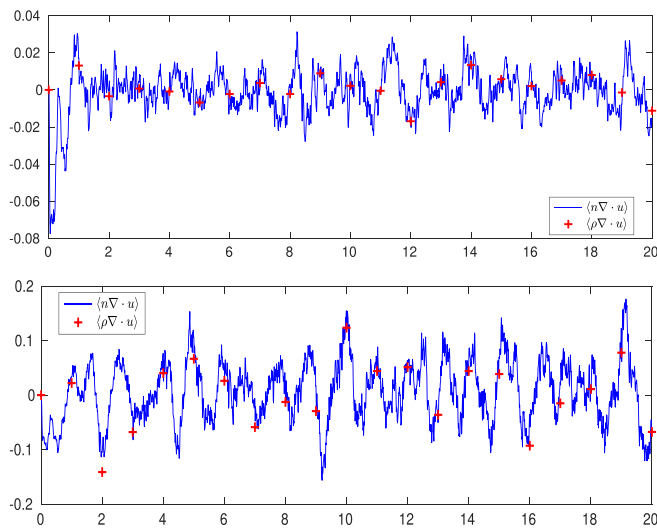


**FIG. 7.** Comparison of weighted dilations. Top: A ST forcing case with  $Re_\lambda = 80$ ,  $M_t = 0.8$ ; Bottom: A C1 forcing case with  $Re_\lambda = 80$ ,  $M_t = 0.8$ .

We first divide the range of  $\rho$ :  $[\rho_{\min}, \rho_{\max}]$  into 100 regions  $[\rho_i, \rho_{i+1}]$ ,  $i = 0, \dots, 99$ . The volume of the domain has a density  $\rho(\mathbf{x})$  in the range  $[\rho_i, \rho_{i+1}]$  is given by  $V_i = \text{Vol}(\{\mathbf{x} | \rho_i < \rho(\mathbf{x}) \leq \rho_{i+1}\})$ . Then, the fluid mass in  $V_i$  is approximately given by  $\bar{\rho}_i V_i$ , where  $\bar{\rho}_i = \frac{\rho_i + \rho_{i+1}}{2}$ . Then, we count the number of particles in  $V_i$  to make the comparison. Such an approach can get results with smaller fluctuations. We introduce  $10^5$  particles into the system at  $t = 5$  with a uniform initial distribution. The results are presented in Fig. 8, from which we see that even though the distributions of  $\rho$  and  $n$  at  $t = 5$  (the starting time) are different, they evolve into almost exactly the same distribution at  $t = 10$ . This result is consistent with the Birkhoff ergodic theorem.<sup>71</sup>

To further verify that the fluid density  $\rho$  and particle number density  $n$  have the same invariant distribution, we tested an extreme case, where the particles are initialized in a small corner of the computational box:  $\{0 \leq x < L/10, 0 \leq y < L/10, 0 \leq z < L/10\}$ . The average particle density  $n$  vs fluid density  $\rho$  in  $V_i$  are plotted in Fig. 9, from which we see, at the very beginning ( $t = 5$ ), the two average densities are very different, but at a later time ( $t = 20$ ), they are linearly correlated.

### D. Spectrum of LEs

Now, we present the results of the probability density functions (PDFs) of calculated LEs and the sum of all three LEs in Figs. 10 and 11, where histogram and fitted normal distribution of calculated LEs and the sum of LEs using different methods are plotted. The simulation time period is  $t = 20 \approx 15T_e \approx 150\tau_\eta$ .  $N = 10^5$  particles are tracked to generate the histogram. We tested taking  $N = 10^4, 10^5, 10^6$  particles, and the difference is very small. We see the PDFs of all three LEs are close to normal distributions. The results of using two different methods for  $\lambda_3$  agree with each other very well. We notice that, even though  $\lambda_2$  has smaller average values than  $\lambda_1$ , its variance is larger. The sums of LEs obtained using two different methods all have much smaller average values and variance than  $\lambda_i$ ,  $i = 1, 2, 3$ , which confirms the fact that the sum of all LEs should be 0.

With similar other parameters used, we see that the ST forcing case has a smaller absolute value of  $\sum \lambda_i$  than the C1 forcing case. This is due to the fact the density variations are larger in the C1 case, which can be verified by the corresponding PDF plots of  $-\ln \rho/t$  in Figs. 10 and 11. More passive particles will stay near high-density regions according to the invariant measure even though the initial distribution is uniform.

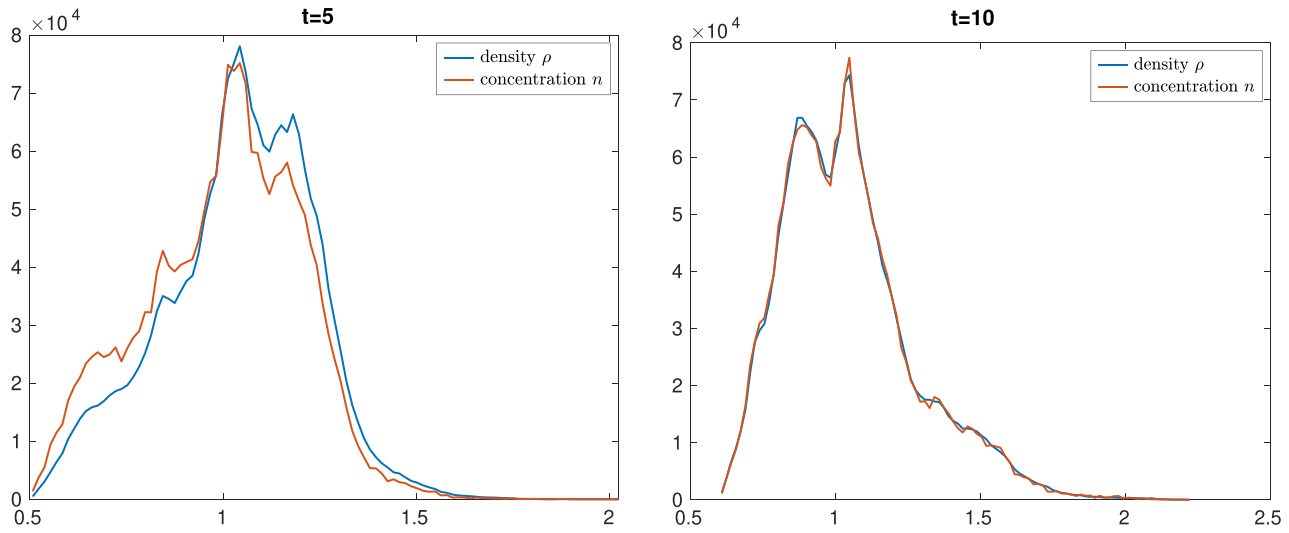


FIG. 8. Direct comparison of  $\rho$  and  $n$ : Mass in different density  $\rho$  regions. Left:  $T = 5$  and right:  $T = 10$ .

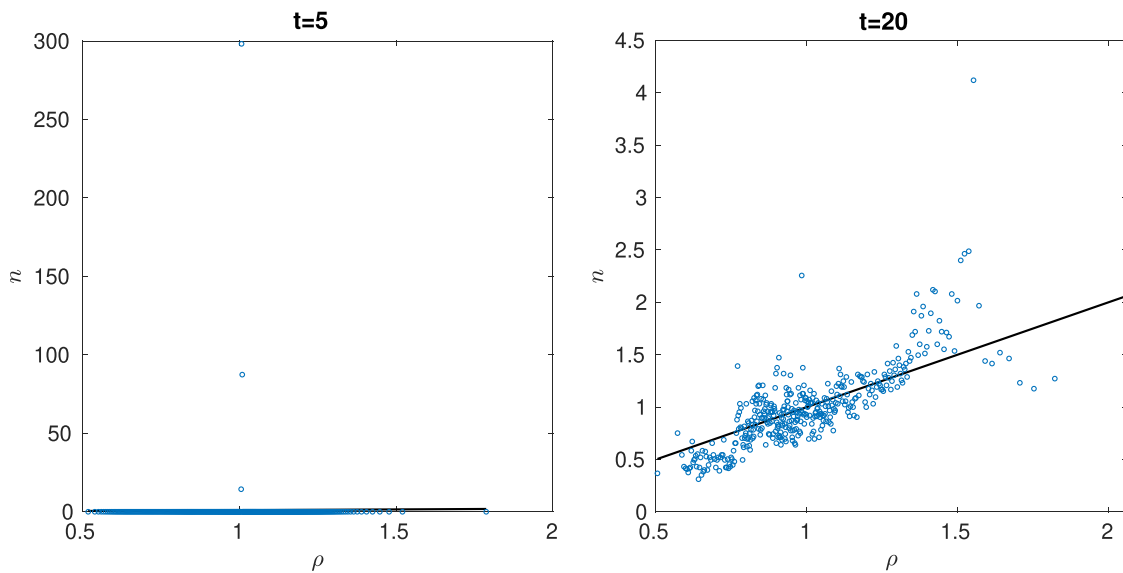


FIG. 9. Direct comparison of the averaged particle density and fluid density in  $V_i$  in an extreme case. Left:  $T = 5$  and right:  $T = 20$ .

### E. Dependence of LEs on turbulent Mach number and Taylor Reynolds number

We show the dependence of  $\lambda_1$  and  $\lambda_2$  on turbulent Mach number  $M_t$  and Taylor Reynolds number  $Re_\lambda$  in Figs. 12 and 13.

In Fig. 12, we see that  $\lambda_1 \tau_\eta$  is a decreasing function of  $M_t$  for both ST and C1 forcing cases. We attribute this to the fact that particles in velocity field with larger compressible components tend to steady clustered near shocks,<sup>42,72</sup> which decreases the separation rate, since larger  $M_t$  and mixed forcing leads to larger  $\delta$ , the ratio of the compressible (dilatational) rms. velocity to solenoidal rms. velocity  $u_{rms}^c/u_{rms}^s$ . The quantity  $\delta$  has been studied as an additional non-dimensional

parameter to get some universal scaling laws of compressible HIT by Donzis and John.<sup>73</sup>

We also observe that the quantity  $\lambda_1 \tau_\eta$  is almost independent of  $Re_\lambda$  (except for  $Re_\lambda = 40$ ) in the ST forcing case for  $1 \geq M_t \geq 0.2$  but has a nearly linear dependence for the C1 forcing case when  $M_t \leq 0.8$ . For  $M_t = 0.2$ , the results of the ST forcing case shown in Fig. 12 that  $\lambda_1 \tau_\eta$  decreases slowly as  $Re_\lambda$  increases, which is consistent with the incompressible flow case (see, e.g., Fig. 7 in Donzis *et al.*<sup>74</sup> and the results in Fouxon *et al.*<sup>29</sup>). We numerically experience that when  $Re_\lambda$  is small, simulations give large variations in  $\lambda_1 \tau_\eta$ . This is because the flow is not fully developed turbulence, and the long time average is

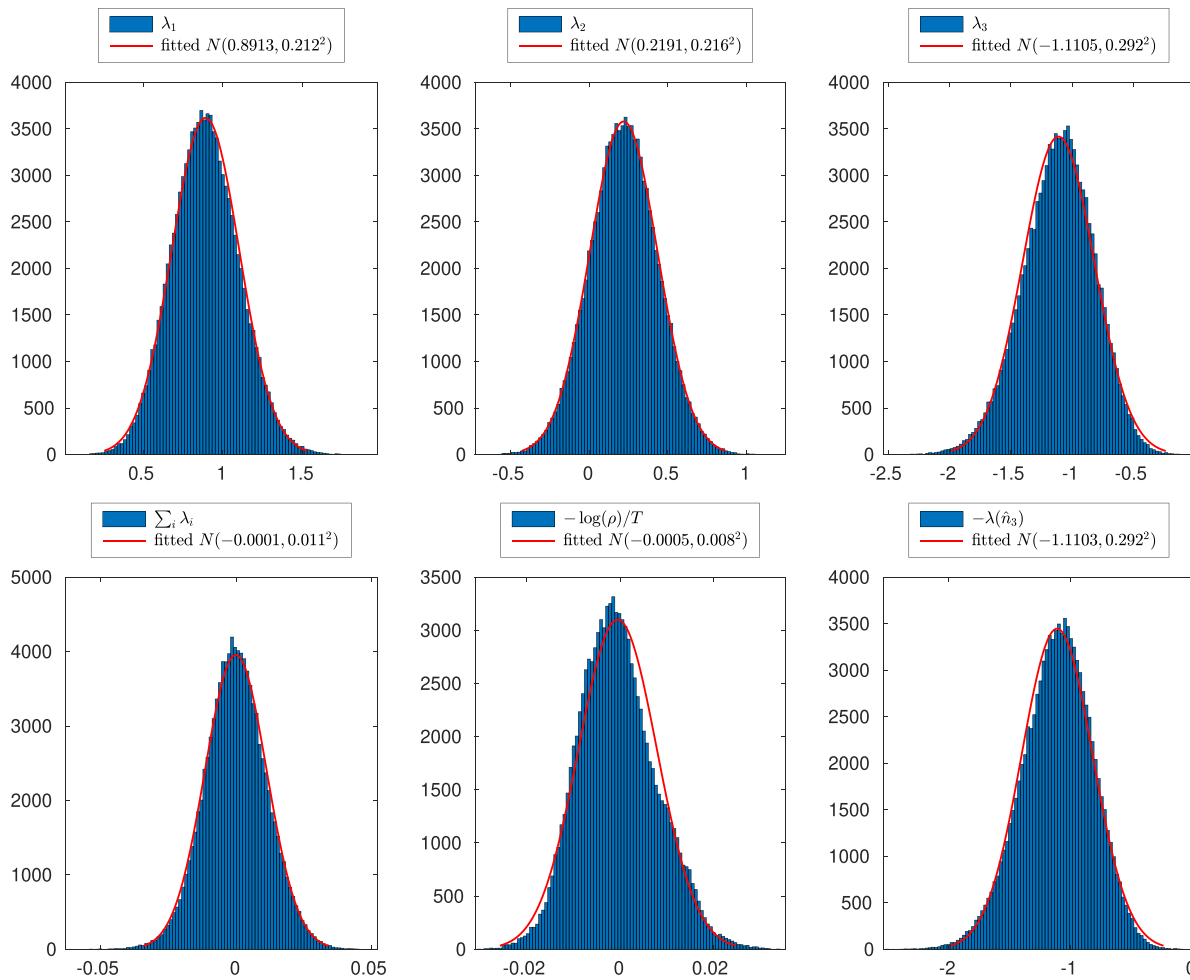


FIG. 10. The distributions of calculated LEs and sum of LEs for the case ST-Re80M06 with solenoidal forcing. The last plot is the  $\lambda_3$  calculated using approach (19).

required to get rid of the chaotic oscillations in the dynamics of Navier–Stokes equations. Therefore, the numerical results reported for  $Re_\lambda \approx 40$  are subject to larger fluctuation errors. Note that Bec *et al.*<sup>75</sup> report  $\lambda_1 \tau_\eta \approx 0.15$  for incompressible turbulence with  $Re_\lambda = 65, 105, 185$ , which is slightly higher than our result interpolated at  $M_t = 0$ .

In Fig. 13, the dependence of  $\lambda_1/\lambda_2$  on Taylor Reynolds number  $Re_\lambda$  and turbulent Mach number  $M_t$  are plotted for the ST and C1 forcing. We see that in ST cases,  $\lambda_1/\lambda_2$  is a decreasing function of  $Re_\lambda$ . In the C1 cases,  $\lambda_1/\lambda_2$  is also a decreasing function of  $Re_\lambda$ , but when  $Re_\lambda$  gets larger, the dependence  $\lambda_1/\lambda_2$  on  $Re_\lambda$  weakens quicker. Due to the fact  $\lambda_2$  is an indicator of time reversibility, smaller values of  $\lambda_1/\lambda_2$  suggest a stronger irreversibility, thus suggesting that the turbulent attractor gets more and more strange as  $Re_\lambda$  increases. For  $Re_\lambda > 80$ , the value  $\lambda_1/\lambda_2$  seems to reach fixed values, which suggests that the flow is close to fully developed turbulence. In particular, for the ST forcing, when  $Re_\lambda \approx 100$ , we observe that  $\lambda_1 : \lambda_2 : \lambda_3 \approx 4 : 1 : -5$ , which is similar to the known result for the incompressible Navier–Stokes system.<sup>30</sup>

In the ST forcing case, the dependence on  $M_t$  is very weak, but in the C1 case, higher  $M_t$  leads to smaller values of  $\lambda_1/\lambda_2$ . When  $M_t$  is close to 1, the ratio  $\lambda_1/\lambda_2$  is smaller than 4.

From the above-mentioned results, we see the dimensionless LEs depend on turbulent Mach number and Taylor Reynolds number nonlinearly. The scaling law is not universal; in other words, it depends on the driving force as well. We note that Donzis and John<sup>73</sup> have introduced  $\delta = u_{rms}^c/u_{rms}^d$  to derive universal scaling laws for compressible turbulence. However, we checked that the relationship between dimensionless LEs and  $\delta$  is not linear either. Since the LEs depend on the dissipation  $\sqrt{\langle |\nabla \mathbf{u}|^2 \rangle}$  rather than energy  $\langle |\mathbf{u}|^2 \rangle$ , we divide  $\sqrt{\langle |\nabla \mathbf{u}|^2 \rangle}$  into the compressible part and solenoidal part and define the ratio of dilation-to-vorticity (in magnitude) as

$$r_{dv} = \sqrt{\langle |\nabla \cdot \mathbf{u}|^2 \rangle / \langle |\nabla \times \mathbf{u}|^2 \rangle}. \tag{26}$$

Figure 14 shows how  $r_{dv}$  depends on turbulent Mach number and Taylor scale Reynolds number. Again, we see a nonlinear relation. The  $Re_\lambda = 40$  in ST forcing case has a quite different scaling because

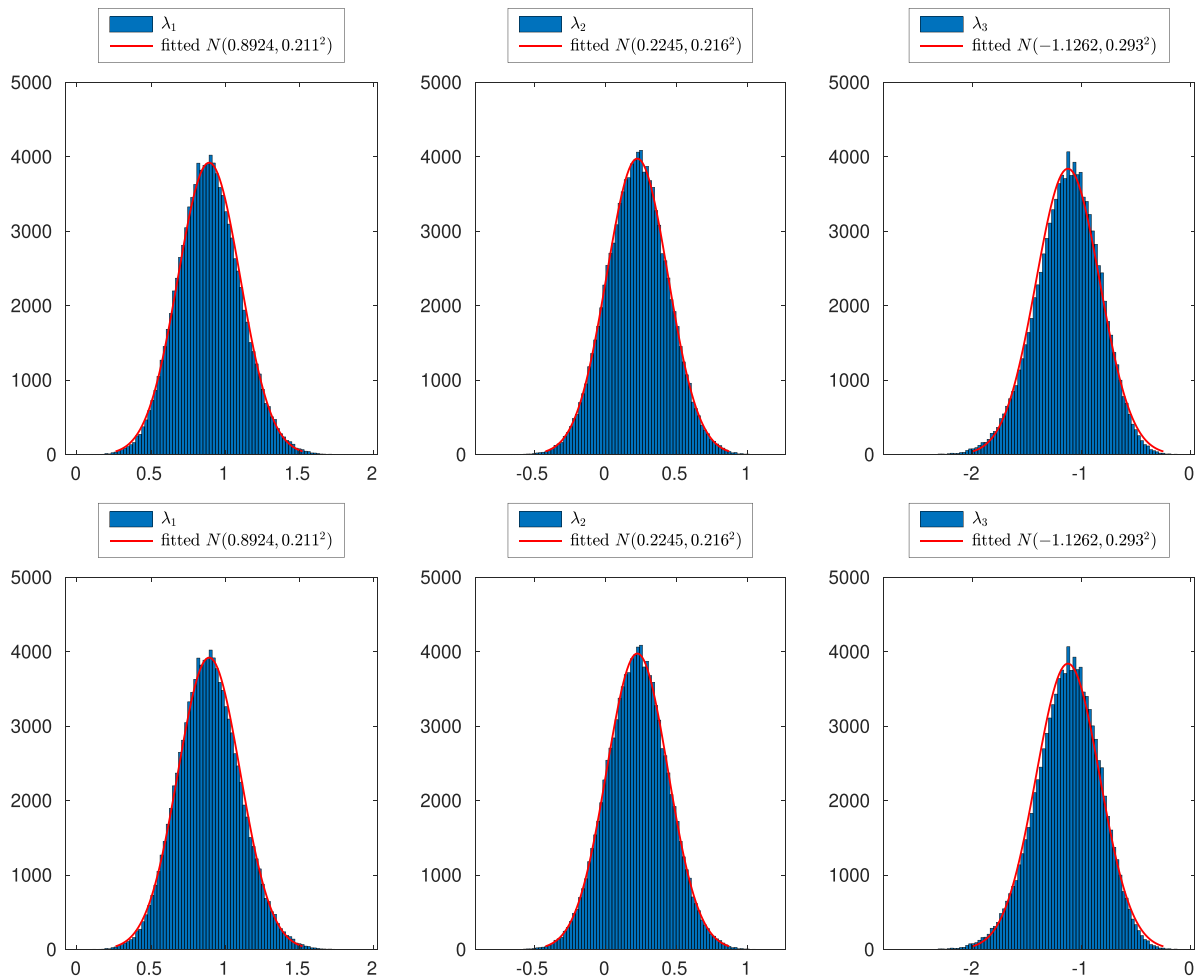


FIG. 11. The distributions of LEs and the sum of LEs for the case C1-Re80M06.

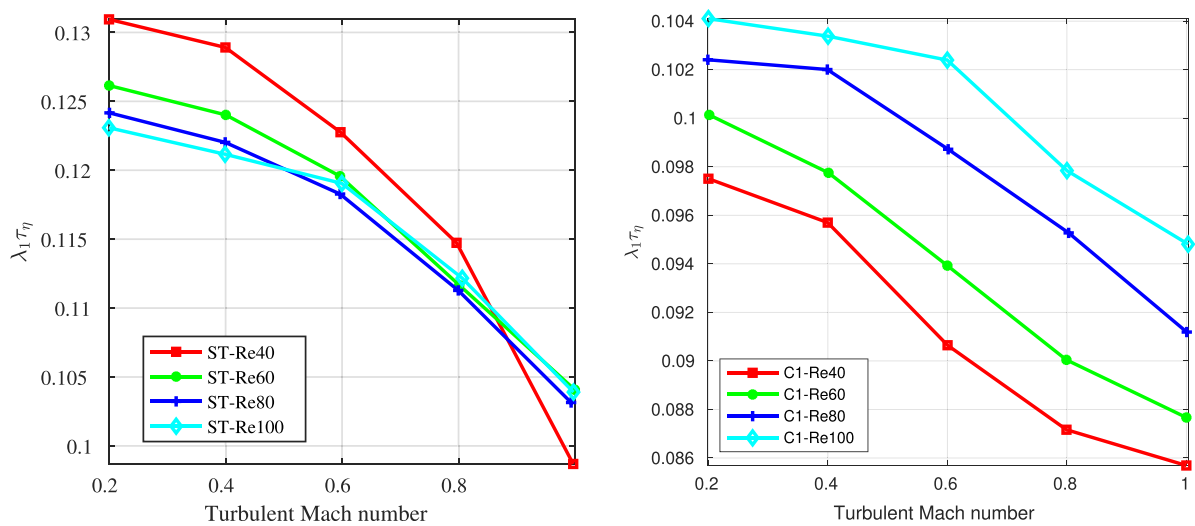


FIG. 12. The relation between  $\lambda_1 \tau_\eta$  and Taylor scale Reynolds number  $Re_\tau$  and turbulent Mach number. Left: solenoidal forcing (ST) and right: mixed forcing (C1).

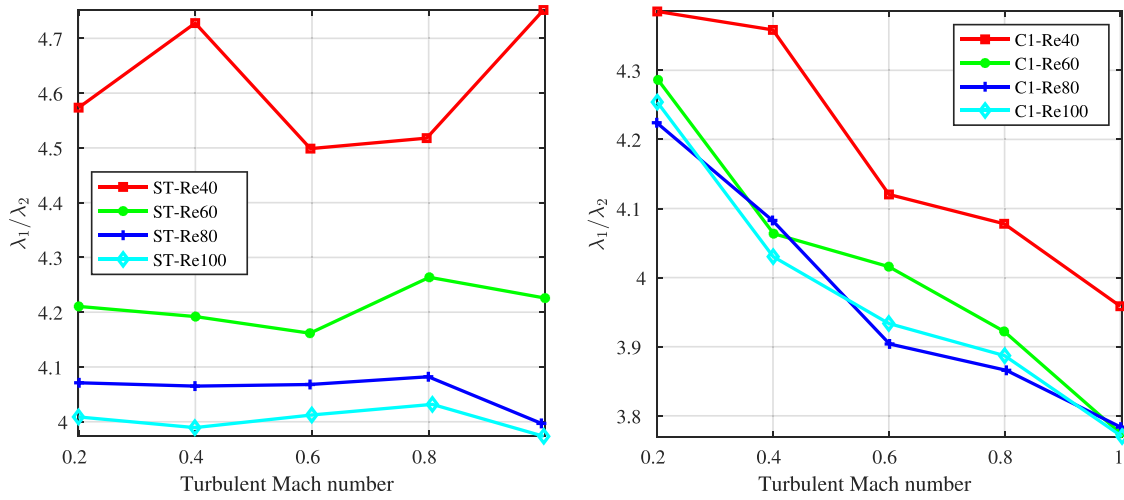


FIG. 13.  $\lambda_1/\lambda_2$  vs Taylor scale Reynolds number and turbulent Mach number. Left: solenoidal forcing (ST) and right: mixed forcing (C1).

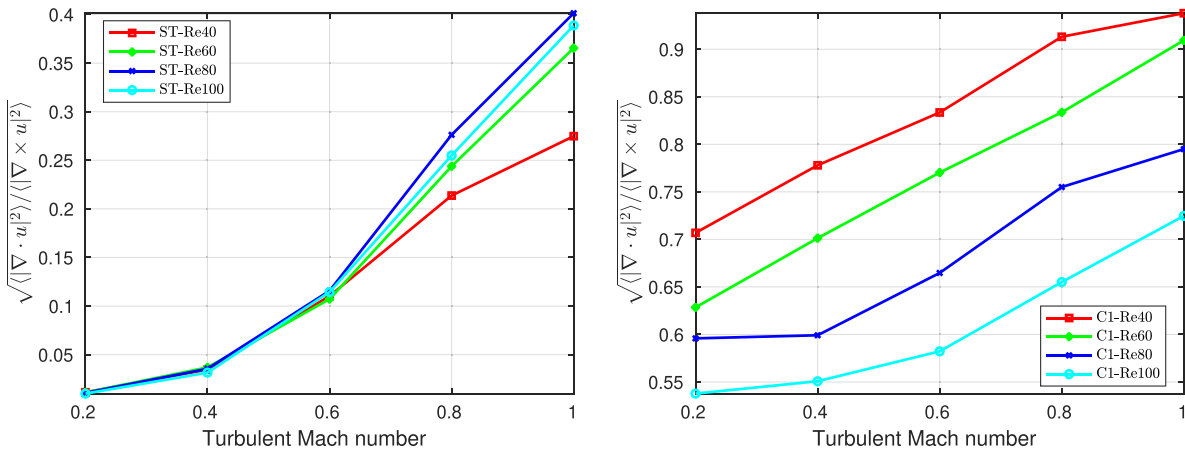


FIG. 14. The ratio of dilation-to-vorticity in magnitude  $r_{dv}$  defined in Eq. (26) as a function of turbulent Mach number and Taylor scale Reynolds number. Left: ST forcing and right: C1 forcing.

the Reynolds number is very small, and the system is too dissipative to allow small-scale compressible velocity to be excited.

Next, we show that the dimensionless LEs depend on  $r_{dv}$  linearly for both ST and C1 forcing cases in Fig. 15, where nine  $M_t$  values (0.2, 0.3, ..., 0.9, 1) are simulated for each  $Re_\lambda$ . From this figure, we see that the linear fitting presents very good results for all Taylor scale Reynolds numbers except for  $Re_\lambda \approx 40$ , and the slopes in ST and C1 forcing cases are very close.

To see clearly the dependence on  $Re_\lambda$ , we carry out a linear fitting for  $Re_\lambda = 60, 80, 100$  separately and present the results of  $\lambda_1 \tau_\eta$  in Fig. 16, where temporal fluctuations of  $\tau_\eta$  in the numerical simulation is used to plot error bars. From this figure, we observe that the slopes and intercepts at different Taylor scale Reynolds numbers and forcing cases are very close (see Fig. 17), which suggests that  $r_{dv}$  is a universal nondimensional parameter for LEs. The results of linear fitting for  $\lambda_3 \tau_\eta$  are similar and not presented.

To give a better understanding of the dilation parts and vorticity parts in  $\nabla \mathbf{u}$ , we give the isosurfaces of the dilation  $\nabla \cdot \mathbf{u}$  and the Frobenius norm of  $|\nabla \mathbf{u}|$  in Fig. 18. If the driving force contains no compressible part, then the dilation component in the velocity gradient is not easy to be excited, even at relatively high  $M_t$  [cf. Figures 18(a) and 18(b)], the correlation between high dilation region and high  $|\nabla \mathbf{u}|$  region is weak. This explains why the dependence of  $\lambda_1/\lambda_2$  on  $M_t$  is weak in solenoidal forcing cases, since the linear fittings of  $\lambda_1 \tau_\eta$  and  $\lambda_2 \tau_\eta$  with respect to  $r_{dv}$  have intercepts much larger than the slopes; meanwhile,  $r_{dv}$  is small. However, in the C1 forcing case, even  $M_t$  is as small as 0.4, the dilation component is dominant in the high-frequency (i.e., small scale) parts [cf. Figures 18(c) and 18(d)]. In other words, the dilation component is responsible for the small-scale variations, which is the major thing to define the LEs. We note that when dilation components are dominant locally, sheet-like structures (thin but broader) corresponding to large-scale shock waves are observed.

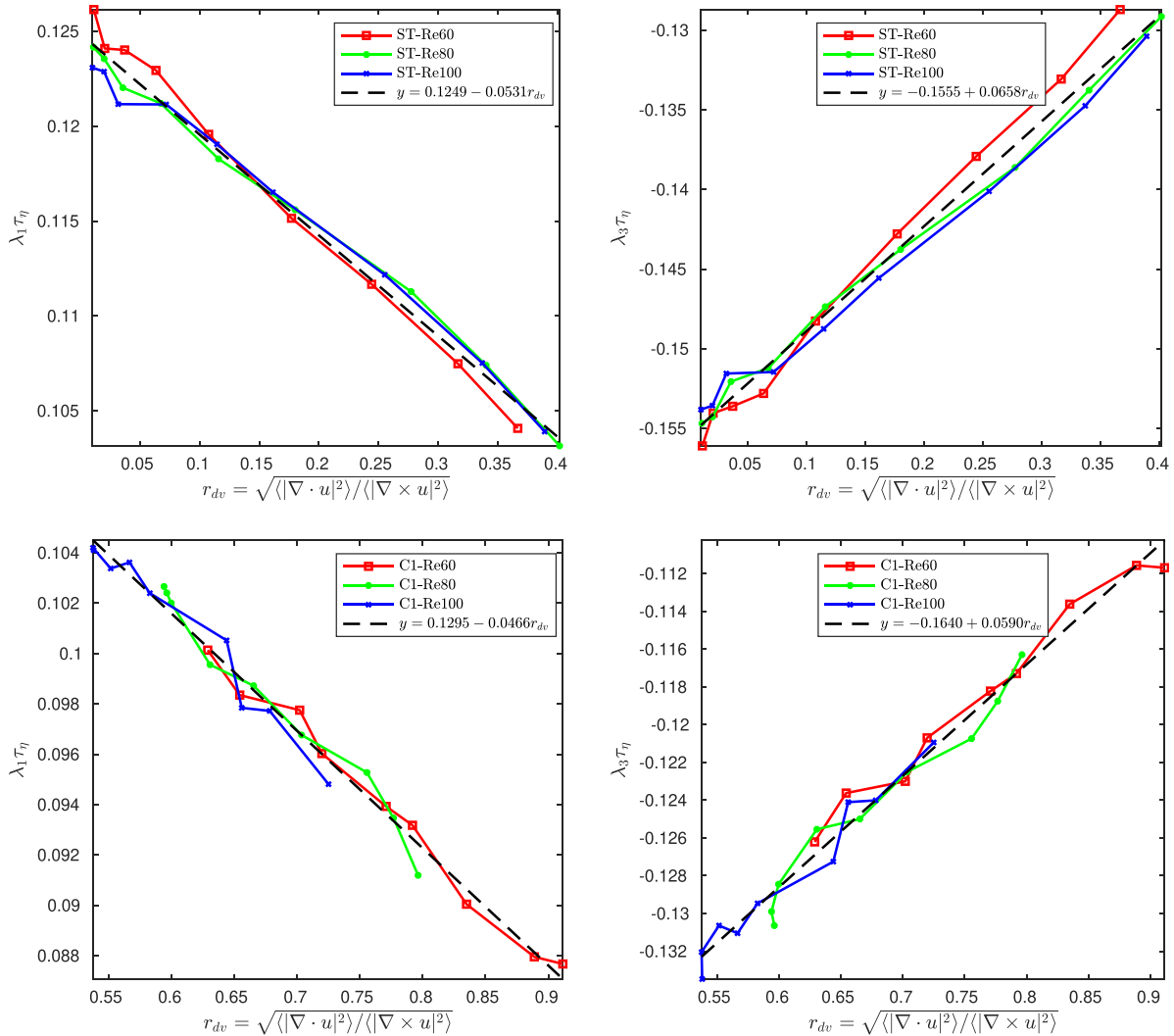


**FIG. 15.** The linear fitting of LEs as functions of  $r_{dv}$  defined in Eq. (26) for different Taylor scale Reynolds numbers. TL: fit  $\lambda_1 \tau_\eta$  for ST forcing; TR: fit  $\lambda_3 \tau_\eta$  for ST forcing; BL: fit  $\lambda_1 \tau_\eta$  for C1 forcing; and BR: fit  $\lambda_3 \tau_\eta$  for C1 forcing.

When vorticity components are dominant, small-scale vortex structures and shocklets are observed.

**VI. CONCLUSIONS**

We developed the theory of statistics of finite-time Lyapunov exponents of compressible turbulence and have carried out a thorough numerical study of Lyapunov exponents of passive particles in compressible homogeneous isotropic turbulence, with emphasis on their dependence on turbulent Mach number and Taylor scale Reynolds number, as well as external forcing.

Our main theoretical result is the general form of the distribution of the finite-time Lyapunov exponents given by Eqs. (21) and (22). For most purposes, the distribution has the same general form as in incompressible flow.<sup>10</sup> This conclusion generalizes the previous observation that the sum of Lyapunov exponents vanishes in compressible turbulence.<sup>11,43</sup> It is remarkable that despite that the flow can have a possibly

large Mach number, the small-scale mixing is effectively incompressible. The role of the Mach number seems mainly to suppress Lagrangian chaos and, consequently, mixing. We observed numerically that both the principal exponent of the Lagrangian flow  $\lambda_1$  and its counterpart for the time-reversed flow  $|\lambda_3|$  decrease with Mach number.

To the best of our knowledge, no numerical study of the Lyapunov exponents of compressible turbulence has been previously published besides Ref. 47. This reference, however, provided estimates of the Lyapunov exponents that do not sum to zero as they should. We believe that the discrepancy is caused by using velocity gradients that are not fully resolved and are effectively coarse-grained. Thus, in our numerical simulations, we paid great attention to achieving the necessary resolution. In contrast to Ref. 47 whose simulations are performed at zero viscosity, our numerical scheme has a finite viscosity. To resolve the shocks, we focused on the middle range of Taylor scale Reynolds

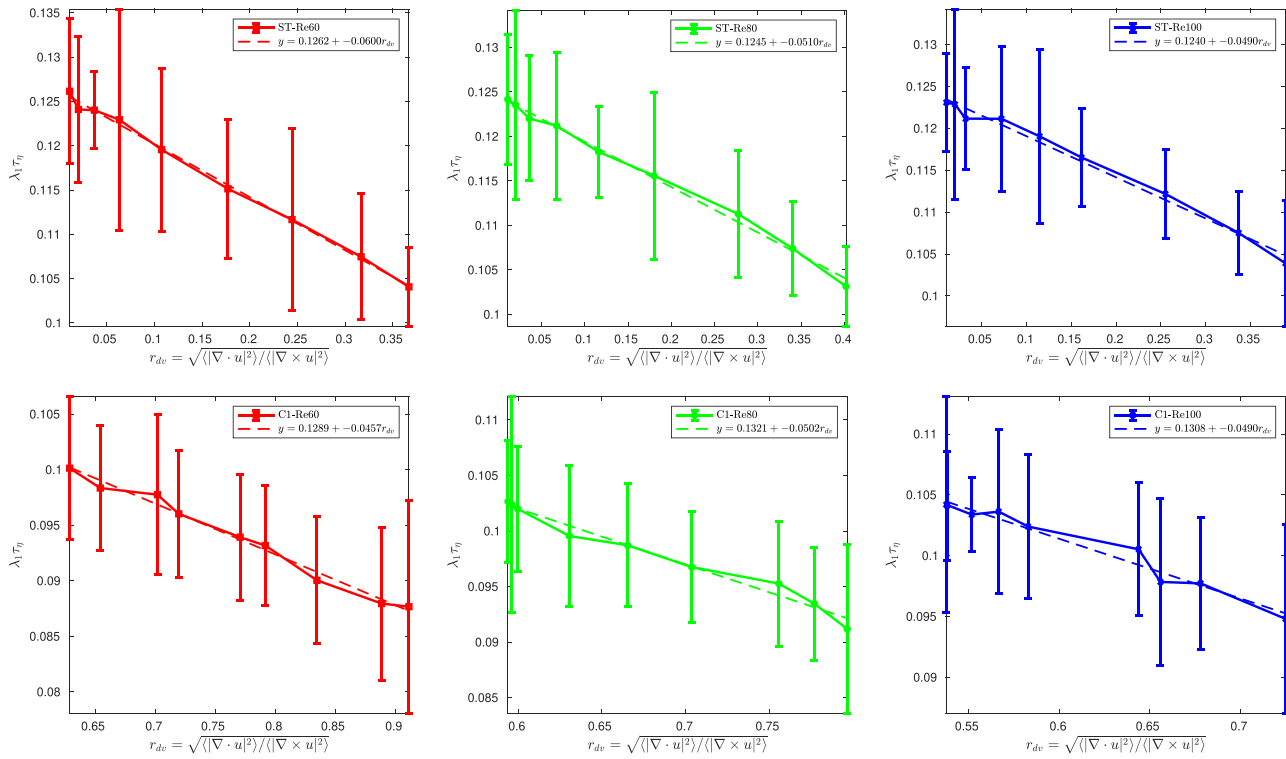


**FIG. 16.** The linear fitting of  $\lambda_1 \tau_\eta$  as functions of  $r_{dv}$  defined in Eq. (26) for different Taylor scale Reynolds numbers. Error bars reflect fluctuations in calculating  $\tau_\eta$ . Top row: fit  $\lambda_1 \tau_\eta$  for ST forcing,  $Re_\lambda = 60$  (left), 80 (middle), and 100 (right); bottom row: fit  $\lambda_1 \tau_\eta$  for C1 forcing with  $Re_\lambda = 60$  (left), 80 (middle), and 100 (right).

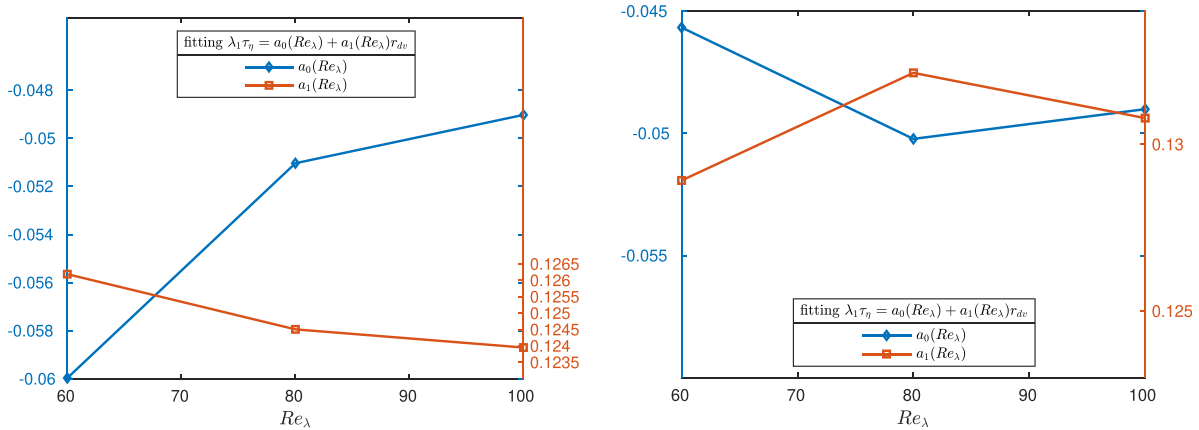


**FIG. 17.** The results of fitting  $\lambda_1 \tau_\eta = a_0(Re_\lambda) + a_1(Re_\lambda)r_{dv}$  for ST forcing (left) and C1 forcing (right).

numbers and adopted high-order numerical schemes. Our findings can be summarized as follows.

- We numerically verified that the sum of LEs of passive particles in compressible turbulence is zero. To get this result, accurate numerical methods and long-time simulation were employed.
- For the solenoidal driving force with  $Re_\lambda > 80$ , we found  $\lambda_1 : \lambda_2 : \lambda_3 \approx 4 : 1 : -5$  that is similar to the incompressible Navier–Stokes system.<sup>30</sup>
- The dependence of  $\lambda_1 \tau_\eta$ ,  $\lambda_1/\lambda_2$  on turbulent Mach number and Taylor Reynolds number is heavily affected by the type of external force.

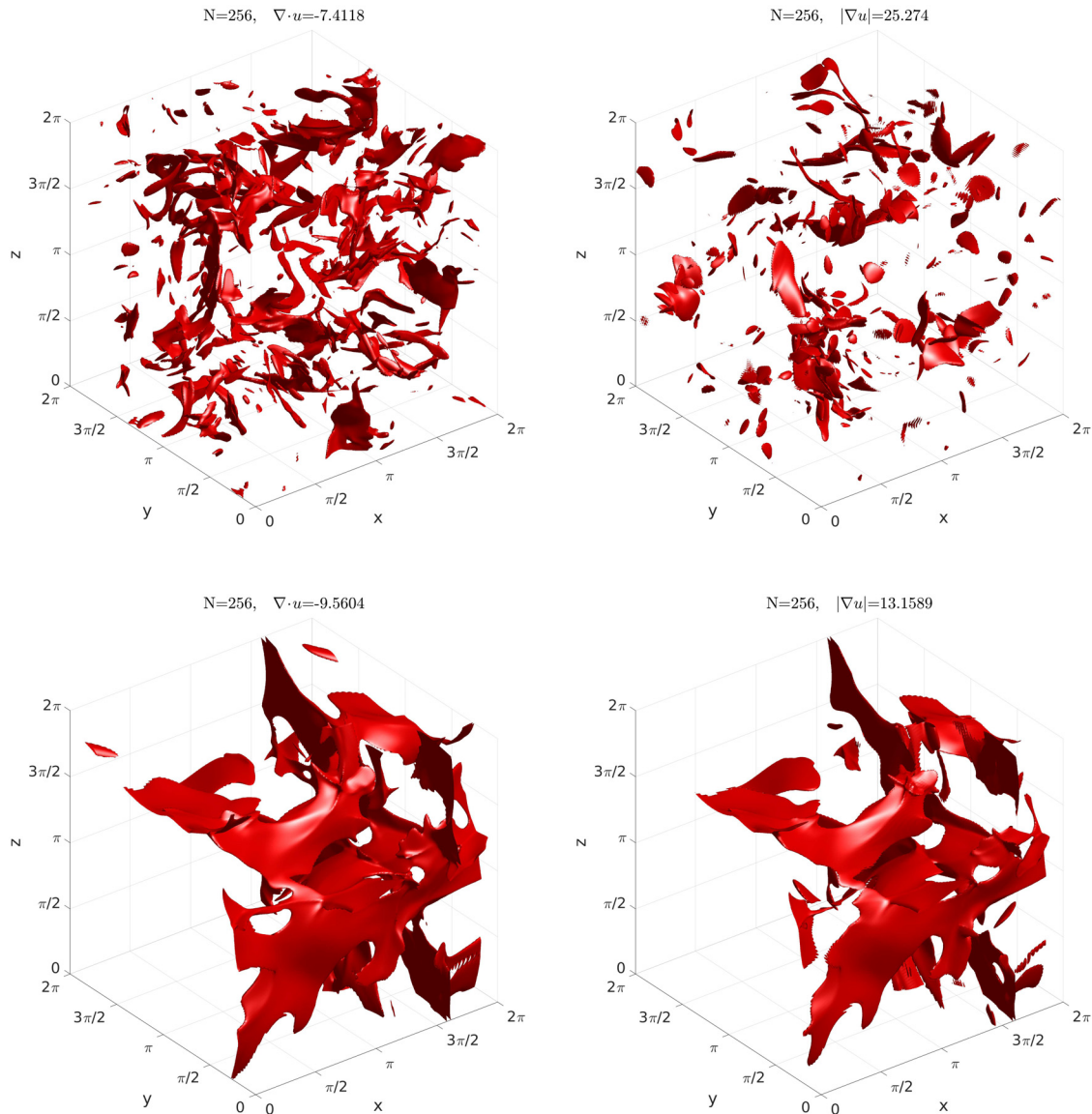


**FIG. 18.** Different correspondence between  $|\nabla \cdot u|$  and  $|\nabla u|$  in different driving forces. TL: ST-Re100M08, dilation; TR: ST-Re100M08,  $|\nabla u|$ ; BL: C1-Re40M04, dilation; and BR: C1-Re40M04,  $|\nabla u|$ .

- We find that the dilation-to-vorticity ratio  $r_{dv} = \sqrt{\langle |\nabla \cdot \mathbf{u}|^2 \rangle / \langle |\nabla \times \mathbf{u}|^2 \rangle}$  is directly responsible for the behavior of dimensionless LEs, which can be used as a control parameter.

We note that there are some limitations to the current work. First, due to the limitation of computational resources, we only investigated a special type of external forcing, although it has been extensively used in the literature. Further investigations with other types of driving force should be performed in order to find out whether  $r_{dv}$  is, indeed, a universal parameter. Second, the numerical error of small Reynolds number  $Re_\lambda \leq 40$  and small Mach number  $M_t \leq 0.2$  may have an undesirable effect, since the numerical scheme we used is not designed

for small  $Re_\lambda$  and small  $M_t$ . Third, this study is limited to  $M_t \leq 1$ . It would also be of interest to study the large deviation function that governs the distribution of the finite-time Lyapunov exponents. Performing this task and going beyond the considered special cases deserves further study.

**ACKNOWLEDGMENTS**

The computations were partially done on the high-performance computers of the State Key Laboratory of Scientific and Engineering Computing, Chinese Academy of Sciences. This work was financially supported by the National Natural Science Foundation of China (Grant No. 12161141017) and the Israel

12 December 2023 01:59:48

Science Foundation (Grant No. 3557/21). H.Y. was also partially supported by NSFC (Grant No. 12171467). L.Y. was partially supported by NSFC (Grant No. 12071470). S.M. was partially supported by NSFC (Grant No. 12271514).

## AUTHOR DECLARATIONS

### Conflict of Interest

The authors have no conflicts to disclose.

### Author Contributions

**Haijun Yu:** Conceptualization (equal); Formal analysis (equal); Funding acquisition (equal); Methodology (equal); Project administration (equal); Resources (equal); Supervision (equal); Visualization (equal); Writing – original draft (equal); Writing – review & editing (equal). **Itzhak Fouxon:** Conceptualization (equal); Formal analysis (equal); Methodology (equal); Writing – review & editing (equal). **Jianchun Wang:** Conceptualization (equal); Methodology (equal); Software (equal); Writing – review & editing (equal). **Xiangru Li:** Data curation (equal); Software (equal); Visualization (equal); Writing – original draft (supporting); Writing – review & editing (supporting). **Li Yuan:** Conceptualization (equal); Methodology (equal); Writing – review & editing (equal). **Shipeng Mao:** Writing – review & editing (equal). **Michael Mond:** Conceptualization (equal); Funding acquisition (equal); Investigation (equal); Methodology (equal); Project administration (equal); Supervision (equal); Writing – review & editing (equal).

### DATA AVAILABILITY

The data that support the findings of this study are available from the corresponding authors upon reasonable request.

### REFERENCES

- <sup>1</sup>E. N. Lorenz, “Deterministic nonperiodic flow,” *J. Atmos. Sci.* **20**, 130–141 (1963).
- <sup>2</sup>T. Nagashima and I. Shimada, “On the C-system-like property of the Lorenz system,” *Prog. Theor. Phys.* **58**, 1318–1320 (1977).
- <sup>3</sup>G. Haller and G. Yuan, “Lagrangian coherent structures and mixing in two-dimensional turbulence,” *Physica D* **147**, 352–370 (2000).
- <sup>4</sup>G. Haller, “Distinguished material surfaces and coherent structures in three-dimensional fluid flows,” *Physica D* **149**, 248–277 (2001).
- <sup>5</sup>A. Hadjighasem, M. Farazmand, D. Blazeviski, G. Froyland, and G. Haller, “A critical comparison of Lagrangian methods for coherent structure detection,” *Chaos* **27**, 053104 (2017).
- <sup>6</sup>X. Ma, Z. Tang, and N. Jiang, “Eulerian and Lagrangian analysis of coherent structures in separated shear flow by time-resolved particle image velocimetry,” *Phys. Fluids* **32**, 065101 (2020).
- <sup>7</sup>S.-L. Cao, X. Sun, J.-Z. Zhang, and Y.-X. Zhang, “Forced convection heat transfer around a circular cylinder in laminar flow: An insight from Lagrangian coherent structures,” *Phys. Fluids* **33**, 067104 (2021).
- <sup>8</sup>S. Yuan, M. Zhou, T. Peng, Q. Li, and F. Jiang, “An investigation of chaotic mixing behavior in a planar microfluidic mixer,” *Phys. Fluids* **34**, 032007 (2022).
- <sup>9</sup>Y. Wu, R. Tao, Z. Yao, R. Xiao, and F. Wang, “Analysis of low-order modal coherent structures in cavitation flow field based on dynamic mode decomposition and finite-time Lyapunov exponent,” *Phys. Fluids* **35**, 085110 (2023).
- <sup>10</sup>E. Balkovsky and A. Fouxon, “Universal long-time properties of Lagrangian statistics in the Batchelor regime and their application to the passive scalar problem,” *Phys. Rev. E* **60**, 4164–4174 (1999).
- <sup>11</sup>G. Falkovich, K. Gawędzki, and M. Vergassola, “Particles and fields in fluid turbulence,” *Rev. Mod. Phys.* **73**, 913–975 (2001).
- <sup>12</sup>G. Boffetta and S. Musacchio, “Chaos and predictability of homogeneous-isotropic turbulence,” *Phys. Rev. Lett.* **119**, 054102 (2017).
- <sup>13</sup>P. Mohan, N. Fitzsimmons, and R. D. Moser, “Scaling of Lyapunov exponents in homogeneous isotropic turbulence,” *Phys. Rev. Fluids* **2**, 114606 (2017).
- <sup>14</sup>A. Berera and R. D. J. G. Ho, “Chaotic properties of a turbulent isotropic fluid,” *Phys. Rev. Lett.* **120**, 024101 (2018).
- <sup>15</sup>U. Frisch, *Turbulence: The Legacy of an Kolmogorov* (Cambridge University Press, Cambridge, 1995).
- <sup>16</sup>D. Ruelle, “Microscopic fluctuations and turbulence,” *Phys. Lett. A* **72**, 81 (1979).
- <sup>17</sup>M. Hassanally and V. Raman, “Lyapunov spectrum of forced homogeneous isotropic turbulent flows,” *Phys. Rev. Fluids* **4**, 114608 (2019).
- <sup>18</sup>D. Clark, L. Tarra, and A. Berera, “Chaos and information in two-dimensional turbulence,” *Phys. Rev. Fluids* **5**, 064608 (2020).
- <sup>19</sup>R. Barrio and S. Serrano, “A three-parametric study of the Lorenz model,” *Physica D* **229**, 43–51 (2007).
- <sup>20</sup>H. Yu, X. Tian, W. Ee, and Q. Li, “OnsagerNet: Learning stable and interpretable dynamics using a generalized Onsager principle,” *Phys. Rev. Fluids* **6**, 114402 (2021).
- <sup>21</sup>E. B. Gledzer, “System of hydrodynamic type admitting two quadratic integrals of motion,” *Sov. Phys. Doklady* **18**, 216 (1973).
- <sup>22</sup>M. Yamada and K. Ohkitani, “Lyapunov spectrum of a chaotic model of three-dimensional turbulence,” *J. Phys. Soc. Jpn.* **56**, 4210–4213 (1987).
- <sup>23</sup>K. Ohkitani and M. Yamada, “Temporal intermittency in the energy cascade process and local Lyapunov analysis in fully-developed model turbulence,” *Prog. Theor. Phys.* **81**, 329–341 (1989).
- <sup>24</sup>M. Yamada and K. Ohkitani, “Asymptotic formulas for the Lyapunov spectrum of fully developed shell model turbulence,” *Phys. Rev. E* **57**, R6257–R6260 (1998).
- <sup>25</sup>S. S. Ray and D. Vincenzi, “Elastic turbulence in a shell model of polymer solution,” *Europhys. Lett.* **114**, 44001 (2016).
- <sup>26</sup>S. S. Ray, “Non-intermittent turbulence: Lagrangian chaos and irreversibility,” *Phys. Rev. Fluids* **3**, 072601 (2018).
- <sup>27</sup>S. D. Murugan, D. Kumar, S. Bhattacharjee, and S. S. Ray, “Many-body chaos in thermalized fluids,” *Phys. Rev. Lett.* **127**, 124501 (2021).
- <sup>28</sup>L. D. Landau and E. M. Lifshitz, *Fluid Mechanics*, 2nd ed., Course of Theoretical Physics (Butterworth-Heinemann Ltd., 1987), Vol. 6.
- <sup>29</sup>I. Fouxon, J. Feinberg, P. Käpylä, and M. Mond, “Reynolds number dependence of Lyapunov exponents of turbulence and fluid particles,” *Phys. Rev. E* **103**, 033110 (2021).
- <sup>30</sup>P. L. Johnson and C. Meneveau, “Large-deviation joint statistics of the finite-time Lyapunov spectrum in isotropic turbulence,” *Phys. Fluids* **27**, 085110 (2015).
- <sup>31</sup>M. R. Maxey, “The gravitational settling of aerosol particles in homogeneous turbulence and random flow fields,” *J. Fluid Mech.* **174**, 441–465 (1987).
- <sup>32</sup>I. Fouxon, Y. Park, R. Harduf, and C. Lee, “Inhomogeneous distribution of water droplets in cloud turbulence,” *Phys. Rev. E* **92**, 033001 (2015).
- <sup>33</sup>I. Fouxon, S. Lee, and C. Lee, “Intermittency and collisions of fast sedimenting droplets in turbulence,” *Phys. Rev. Fluids* **7**, 124303 (2022).
- <sup>34</sup>I. Fouxon, G. Shim, S. Lee, and C. Lee, “Multifractality of fine bubbles in turbulence due to lift,” *Phys. Rev. Fluids* **3**, 124303 (2018).
- <sup>35</sup>W. M. Durham, E. Climent, M. Barry, F. De Lillo, G. Boffetta, M. Cencini, and R. Stocker, “Turbulence drives microscale patches of motile phytoplankton,” *Nat. Commun.* **4**, 2148 (2013).
- <sup>36</sup>I. Fouxon and A. Leshansky, “Phytoplankton’s motion in turbulent ocean,” *Phys. Rev. E* **92**, 013017 (2015).
- <sup>37</sup>L. Schmidt, I. Fouxon, D. Krug, M. van Reeuwijk, and M. Holzner, “Clustering of particles in turbulence due to phoresis,” *Phys. Rev. E* **93**, 063110 (2016).
- <sup>38</sup>I. Fouxon, “Distribution of particles and bubbles in turbulence at a small Stokes number,” *Phys. Rev. Lett.* **108**, 134502 (2012).
- <sup>39</sup>G. Falkovich and A. Fouxon, “Entropy production and extraction in dynamical systems and turbulence,” *New J. Phys.* **6**, 50 (2004).
- <sup>40</sup>G. Falkovich, A. Fouxon, and V. M. Stepanov, “Acceleration of rain initiation by cloud turbulence,” *Nature* **419**, 151–154 (2002).

- <sup>41</sup>M. Chertkov, I. Kolokolov, and M. Vergassola, "Inverse versus direct cascades in turbulent advection," *Phys. Rev. Lett.* **80**, 512 (1998).
- <sup>42</sup>K. Gawędzki and M. Vergassola, "Phase transition in the passive scalar advection," *Physica D* **138**, 63–90 (2000).
- <sup>43</sup>I. Fouxon and M. Mond, "Density and tracer statistics in compressible turbulence: Phase transition to multifractality," *Phys. Rev. E* **100**, 023111 (2019).
- <sup>44</sup>I. Fouxon, B. Meerson, M. Assaf, and E. Livne, "Formation of density singularities in ideal hydrodynamics of freely cooling inelastic gases: A family of exact solutions," *Phys. Fluids* **19**, 093303 (2007).
- <sup>45</sup>I. Fouxon, B. Meerson, M. Assaf, and E. Livne, "Formation and evolution of density singularities in hydrodynamics of inelastic gases," *Phys. Rev. E* **75**, 050301 (2007).
- <sup>46</sup>I. Fouxon, "Finite-time collapse and localized states in the dynamics of dissipative gases," *Phys. Rev. E* **80**, 010301 (2009).
- <sup>47</sup>C. Schwarz, C. Beetz, J. Dreher, and R. Grauer, "Lyapunov exponents and information dimension of the mass distribution in turbulent compressible flows," *Phys. Lett. A* **374**, 1039–1042 (2010).
- <sup>48</sup>A. Kurganov and D. Levy, "A third-order semidiscrete central scheme for conservation laws and convection-diffusion equations," *SIAM J. Sci. Comput.* **22**, 1461–1488 (2000).
- <sup>49</sup>C.-W. Shu and S. Osher, "Efficient implementation of essentially non-oscillatory shock-capturing schemes," *J. Comput. Phys.* **77**, 439–471 (1988).
- <sup>50</sup>G. Benettin, L. Galgani, A. Giorgilli, and J.-M. Strelcyn, "Lyapunov characteristic exponents for smooth dynamical systems and for Hamiltonian systems: A method for computing all of them. Part 1: Theory," *Meccanica* **15**, 9–20 (1980).
- <sup>51</sup>J. Wang, L.-P. Wang, Z. Xiao, Y. Shi, and S. Chen, "A hybrid numerical simulation of isotropic compressible turbulence," *J. Comput. Phys.* **229**, 5257–5279 (2010).
- <sup>52</sup>W. Sutherland, "The viscosity of gases and molecular force," *London, Edinburgh, Dublin Philos. Mag. J. Sci.* **36**, 507–531 (1893).
- <sup>53</sup>S. Jagannathan and D. A. Donzis, "Reynolds and Mach number scaling in solenoidally-forced compressible turbulence using high-resolution direct numerical simulations," *J. Fluid Mech.* **789**, 669–707 (2016).
- <sup>54</sup>L. Liu, J. Wang, Y. Shi, S. Chen, and X. T. He, "A hybrid numerical simulation of supersonic isotropic turbulence," *Commun. Comput. Phys.* **25**, 189–217 (2019).
- <sup>55</sup>V. Eswaran and S. B. Pope, "An examination of forcing in direct numerical simulations of turbulence," *Comput. Fluids* **16**, 257–278 (1988).
- <sup>56</sup>S. Kida and S. A. Orszag, "Energy and spectral dynamics in forced compressible turbulence," *J. Sci. Comput.* **5**, 85–125 (1990).
- <sup>57</sup>P. D. Mininni, A. Alexakis, and A. Pouquet, "Large-scale flow effects, energy transfer, and self-similarity on turbulence," *Phys. Rev. E* **74**, 016303 (2006).
- <sup>58</sup>M. R. Petersen and D. Livescu, "Forcing for statistically stationary compressible isotropic turbulence," *Phys. Fluids* **22**, 116101 (2010).
- <sup>59</sup>L. Konstantin, C. Federrath, R. S. Klessen, and W. Schmidt, "Statistical properties of supersonic turbulence in the Lagrangian and Eulerian frameworks," *J. Fluid Mech.* **692**, 183–206 (2012).
- <sup>60</sup>J. P. John, D. A. Donzis, and K. R. Sreenivasan, "Does dissipative anomaly hold for compressible turbulence?," *J. Fluid Mech.* **920**, A20 (2021).
- <sup>61</sup>E. Balkovsky, G. Falkovich, and A. Fouxon, "Intermittent distribution of inertial particles in turbulent flows," *Phys. Rev. Lett.* **86**, 2790 (2001).
- <sup>62</sup>I. Fouxon, S. Ainsaar, and J. Kalda, "Quartic polynomial approximation for fluctuations of separation of trajectories in chaos and correlation dimension," *J. Stat. Mech.* **2019**, 083211.
- <sup>63</sup>J. R. Ristorcelli, "A pseudo-sound constitutive relationship for the dilatational covariances in compressible turbulence," *J. Fluid Mech.* **347**, 37 (1997).
- <sup>64</sup>G. P. Zank and W. H. Matthaeus, "The equations of nearly incompressible fluids, I: Hydrodynamics, turbulence, and waves," *Phys. Fluids A* **3**, 69 (1991).
- <sup>65</sup>S. Sankar, G. Erlebacher, M. Y. Hussaini, and H. O. Kreiss, "The analysis and modeling of dilatational terms in compressible turbulence," *J. Fluid Mech.* **227**, 473 (1991).
- <sup>66</sup>J. Wang, T. Gotoh, and T. Watanabe, "Spectra and statistics in compressible isotropic turbulence," *Phys. Rev. Fluids* **2**, 013403 (2017).
- <sup>67</sup>S. K. Lele, "Compact finite difference schemes with spectral-like resolution," *J. Comput. Phys.* **103**, 16–42 (1992).
- <sup>68</sup>D. S. Balsara and C.-W. Shu, "Monotonicity preserving weighted essentially non-oscillatory schemes with increasingly high order of accuracy," *J. Comput. Phys.* **160**, 405–452 (2000).
- <sup>69</sup>N. A. Adams and K. Shariff, "A high-resolution hybrid compact-ENO scheme for shock-turbulence interaction problems," *J. Comput. Phys.* **127**, 27–51 (1996).
- <sup>70</sup>J.-P. Eckmann and D. Ruelle, "Ergodic theory of chaos and strange attractors," *Rev. Mod. Phys.* **57**, 617 (1985).
- <sup>71</sup>G. D. Birkhoff, "Proof of the Ergodic Theorem," *Proc. Natl. Acad. Sci. U. S. A.* **17**, 656–660 (1931).
- <sup>72</sup>Y. Yang, J. Wang, Y. Shi, Z. Xiao, X. T. He, and S. Chen, "Interactions between inertial particles and shocklets in compressible turbulent flow," *Phys. Fluids* **26**, 091702 (2014).
- <sup>73</sup>D. A. Donzis and J. P. John, "Universality and scaling in homogeneous compressible turbulence," *Phys. Rev. Fluids* **5**, 084609 (2020).
- <sup>74</sup>D. A. Donzis, K. R. Sreenivasan, and P. K. Yeung, "The Batchelor spectrum for mixing of passive scalars in isotropic turbulence," *Flow Turbul. Combust.* **85**, 549–566 (2010).
- <sup>75</sup>J. Bec, L. Biferale, G. Boffetta, M. Cencini, S. Musacchio, and F. Toschi, "Lyapunov exponents of heavy particles in turbulence," *Phys. Fluids* **18**, 091702 (2006).